# Strong correlations in gravity and biophysics

Dmitry Krotov

A Dissertation

Presented to the Faculty

of Princeton University

in Candidacy for the Degree

of Doctor of Philosophy

Recommended for Acceptance

by the Department of

Physics

Advisers: Professors William Bialek and Alexander Polyakov

September 2014

# Abstract

The unifying theme of this dissertation is the use of correlations. In the first part (chapter 2), we investigate correlations in quantum field theories in de Sitter space. In the second part (chapters 3,4,5), we use correlations to investigate a theoretical proposal that real (observed in nature) transcriptional networks of biological organisms are operating at a critical point in their phase diagram.

In chapter 2 we study the infrared dependence of correlators in various external backgrounds. Using the Schwinger-Keldysh formalism we calculate loop corrections to the correlators in the case of the Poincare patch and the complete de Sitter space. In the case of the Poincare patch, the loop correction modifies the behavior of the correlator at large distances. In the case of the complete de Sitter space, the loop correction has a strong dependence on the infrared cutoff in the past. It grows linearly with time, suggesting that at some point the correlations become strong and break the symmetry of the classical background.

In chapter 3 we derive the signatures of critical behavior in a model organism, the embryo of *Drosophila melanogaster*. They are: strong correlations in the fluctuations of different genes, a slowing of dynamics, long range correlations in space, and departures from a Gaussian distribution of these fluctuations. We argue that these signatures are observed experimentally.

In chapter 4 we construct an effective theory for the zero mode in this system. This theory is different from the standard Landau-Ginsburg description. It contains gauge fields (the result of the broken translational symmetry inside the cell), which produce observable contributions to the two-point function of the order parameter. We show that the behavior of the two-point function for the network of $N$ genes is described by the action of a relativistic particle moving on the surface of the $N - 1$ dimensional sphere. We derive a theoretical bound on the decay of the correlations and compare it with experimental data.

How difficult is it to tune a network to criticality? In chapter 5 we construct the space of all possible networks within a simple thermodynamic model of biological enhancers. We demonstrate that there is a reasonable number of models within this framework that accurately capture the mean expression profiles of the gap genes that are observed experimentally.

# Acknowledgements

During my time at Princeton I have been very lucky to have the opportunity to interact with and learn from two communities within the Physics Department: the High Energy Physics Theory group and the Theoretical Biophysics group. I am highly indebted to the members of both of them for making the Physics Department such a great place to develop as a scientist.

In the fall of 2008, my first semester at Princeton, I was fortunate to take a class on Quantum Field Theory taught by my eventual adviser Professor Alexander Polyakov. This was the first time that I was exposed to a completely new level of thinking about this subject, one that went far deeper compared to the textbooks that I used to read before and far broader than just calculating the scattering cross-sections. Highly inspirational discussions after every class led me to my first research project at Princeton, which was related to the infrared properties of quantum field theories in external backgrounds. I worked on this project for three years and absorbed an enormous (on my scale) wealth of methods and tools that are used in various areas of theoretical physics. I would like to thank Alexander Markovich for his generosity in sharing some of his thoughts with me, his dedicated mentoring and his help at every step of the way both with my first project and those that have followed. The ratio of what I knew about theoretical physics before I started working with him to what I (hopefully) know now is almost negligible.

A second pivotal moment in my scientific life was a class on Biophysics taught by a highly inspiring scientist, and also my eventual adviser, Professor William Bialek. Although the idea of working in the field of Biological Sciences had crossed my mind on a few occasions before then, I had never taken it too seriously because of the (incorrect) impression that biology lacks a theoretical approach and the feeling that what is called "theory" in biology is just a tool that helps to quantify a little bit something that was already obvious in advance. I am very thankful to Bill for helping

me understand the crucial role that theory plays in biological research, one that is similar to those it plays in other subfields of physics. I am very grateful to Bill for the many lessons on how to work with biological data, something that I had never done before. His deep vision and a subtle taste to problems in theoretical biophysics have significantly influenced my research interests and will continue to do so in the future.

My very special thanks go to Curtis Callan and Eric Wieschaus for many extremely thought-provoking discussions, careful guidance, and their constant support throughout my time at Princeton.

Finally, I would like to thank my friends and colleagues in the Physics Department and Lewis–Sigler Institute for Integrative Genomics: Ji Hyun Bak, Gordon Berman, Farzan Beroz, Anne-Florence Bitbol, Chase Broedersz, Michele Castellana, Kostya Doubrovinski, Julien Dubuis, John Hopfield, Mark Ioffe, Igor Klebanov, Jeongseog Lee, Ben Machta, Leenoy Meshulam, Vitya Mikhaylov, Anand and Arvind Murugans, Armita Nourmohammad, Miriam Osterfield, Stephanie Palmer, Yeje Park, Guilherme Pimentel, Kanaka Rajan, Zack Sethna, David Schwab, DJ Strouse, Grisha Tarnopolskiy, Thibaud Taillefumier, Misha Tikhonov, Ned Wingreen, and Sasha Zhiboedov.

I consider myself very lucky to have had the opportunity to learn from so many talented and thoughtful scientists during the last six years.

**Publications and preprints associated with this dissertation**

1. D. Krotov and A. M. Polyakov, "Infrared Sensitivity of Unstable Vacua", *Nucl.Phys.* **B849**, 410-432 (2011), arXiv:1012.2107(hep-th).

2. D.Krotov, J.O.Dubuis, T.Gregor, and W.Bialek, "Morphogenesis at criticality", *Proceedings of the National Academy of Sciences*, **111-10**, 3683–3688 (2014), arXiv:1309.2614(q-bio).

Materials from this dissertation have been publicly presented at the following conferences and seminars:

1. American Physical Society March Meeting, Denver, CO (2014)

2. Seminar at Rockefeller University, New York (2014)

3. Seminar at KITP, Santa Barbara (2014)

4. Seminar at SEAS, Harvard University (2013)

5. Seminar at the Simons Center for Systems Biology, IAS, Princeton (2013)

6. Biophysics Seminar, Rutgers University (2013)

7. Q-bio Conference, Santa Fe, NM (2013)

8. NA School of Information Theory, Purdue University, (2013) (poster)

9. American Physical Society March Meeting, Baltimore, MD (2013)

10. Cells, Circuits, and Computation, Harvard University (2013)

11. International Physics of Living Systems: iPoLS, Montpellier, France (2012)

# Contents

# List of Tables

# List of Figures

# Chapter 1

# Introduction

The central theme that runs through this dissertation is the use of correlations. More specifically we[1] discuss two projects. One pertains to the study of quantum fields in de Sitter space, the other one pertains to the study of transcriptional networks in biological organisms. In the first problem the correlators are calculated by averaging over quantum fluctuations, in the second problem they are calculated by averaging over an ensemble of biological cells. In each particular cell of the ensemble the state of the transcriptional network is slightly different, resulting in fluctuations of the concentrations of proteins around their mean values. Just as studying the scattering cross-sections of elementary particles provides information on the underlying lagrangian describing particle interactions, studying the correlations of protein concentrations can help us to elucidate properties of transcriptional networks of real biological cells - a question of crucial importance for our understanding of biological systems.

In both projects we discover correlators that become large in certain situations, and in both projects these correlations persist over long distances. The physical consequences, however, are different. In the case of de Sitter space these long-range

---

[1]Most of the ideas discussed in this dissertation were developed in collaboration. Therefore I use "we" referring to my coauthors and myself.

correlations signal the symmetry breaking of the classical geometry. In the case of biological cells, these strong correlations suggest a theoretical hypothesis that the transcriptional networks we study are operating in the vicinity of critical surfaces in their phase digram.

Below we present two separate introduction sections that more specifically address the questions that we discuss in the two projects. They are presented in chronological order.

## 1.1 Part one. Infrared effects in external fields.

De Sitter space plays a fundamental role in physics. It is a maximally symmetric space, it is important for applications to cosmology, it is important in the context of dS/CFT correspondence, etc. In spite of its crucial role, the quantum field theory on this space conceals many puzzles and confusions. Geometrically, this space can be defined as an analytic continuation from the sphere. Therefore, it is tempting to define the following rules for calculating the quantum correlation functions: first calculate a correlator that we are interested in on the sphere (this is often a simple calculation) and then analytically continue the final answer to the de Sitter space. In certain cases such a recipe works, in others it does not. Therefore, it seems important to me to outline the range of problems where such an analytic continuation is possible and where it is not, and, more importantly, find the correct results for the quantum correlators in those cases when the analytic continuation fails.

Historically the topic of quantum field theories in external backrounds may sound like a relatively old and well developed area of research, that used to be popular in the eighties (see the classical textbook [6] for a review of the field at that time). It is important to emphasize, however, that most of the work on the subject has been done in free theories, leaving aside the effects due to non-linear interactions (which

is the main topic of the present study). The other problem is that even in linear theories, the calculations are quite complicated so that different papers often arrive at opposite conclusions, in part because of subtleties of the analytic continuation from the sphere (see the next section for the specific examples). The situation gets even more complicated if we recall that the de Sitter space has several different coordinate systems that sometimes cover various parts of the whole space. Quantum field theories on these subspaces of the complete de Sitter hyperboloid may look very different from each other and very different from the theory that is obtained by the analytical continuation from the sphere. The first part of the present dissertation is an attempt to address some of the many questions that exist in this field. More specifically, we focus on the theory on the complete de Sitter space and on the Poincare patch of the de Sitter space, which is believed to be relevant for cosmology. Our main results are the existence of infrared corrections to the free Green functions that arise from loop diagrams. We often use a toy-model example of an electric field to illustrate the unusual (from the perspective of conventional, equilibrium, quantum field theory) features of the formalism.

There is a separate, phenomenological, motivation for this work that stems from an attempt to solve the problem of the cosmological constant. The idea is the following [40, 41, 28, 42]: imagine that we start from an empty de Sitter space with some massive field (a scalar field for simplicity) minimally coupled to gravity. In the course of time evolution (expansion of the Universe) the expectation value of the energy-momentum tensor of the scalar field changes with time. It is possible that at some point, in the course of expansion, it becomes large because of the infrared corrections that we study. If this happens, we can no longer treat the metric as a background and must take into account the back reaction of the scalar field on the time evolution of the metric after that moment. There are many steps on the way of turning this proposal into a physical mechanism. Perhaps the first step is to identify the situations when

3

the infrared corrections appear, and, among those cases, the situations when these corrections lead to a strong backreaction that signals the instability of the classical geometry.

Although this phenomenological motivation exists, it is not the main subject of the present dissertation. Our primary goal is theoretical – to investigate the infrared properties of quantum field theories on the de Sitter space.

Most of the results discussed here are published in [28]. These ideas are a development of an earlier proposal [40, 41].

## 1.2   Part two. Criticality in transcriptional networks.

All cells in the body of a multicellular organism contain almost identical DNA, yet cells of different tissues (for example skin cells vs. neurons) are very different. These differences arise because only a fraction of all the proteins encoded in the DNA are expressed in a given cell. What proteins are expressed and what proteins are not is determined by a combination of transcription factors, the proteins that bind to DNA and induce transcription of certain genes. Some of the proteins encoded by the genes that are transcribed are also transcription factors that can influence expression levels of themselves or of other genes. Thus we have a network of proteins whose concentrations are determined by some dynamical equations, and the rate of production of each individual protein depends on the concentrations of all the transcription factors that are part of the network. For different choices of the parameters of these equations, the behavior of the network can be very different. It can have a single steady state, it can have multiple steady states, it can have no steady states at all (leading to persistent oscillations), etc. All these different regimes represent different phases on the phase diagram of the network. Much has been said about genetic networks operating deeply inside any of these phases [50, 13, 48]. In the present dissertation we explore
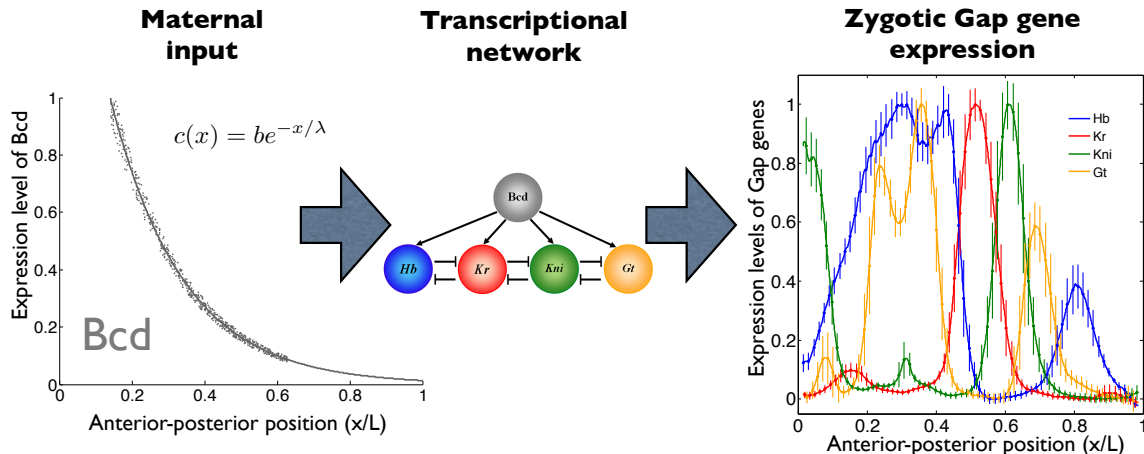
4

Figure 1.1: Left panel shows the anterior-posterior distribution of the Bicoid protein (this is just a cartoon and not the real data), which is one of the transcription factors involved in the patterning of the embryo. The coordinate-dependent profile provides an input to the network of gap genes. These genes are dynamically expressed and interact with each other forming the transcriptional network (this is just a cartoon of the network and not the real network, see [20] for a summary of the known details about the real network). As an output of this network we observe a pattern of gap gene expression profiles. The anterior-posterior dependence of the mean expression profiles is shown on the right panel (data from [11]). The network produces these profiles at the late stage of nuclear cycle 14. The error bars represent variability ($\pm$ standard deviation) of individual profiles around the mean profile.

the possibility that real genetic networks are operating in the vicinity of boundaries between the phases - the critical surfaces. From physical intuition we know that the behavior of the network at criticality is qualitatively different from any of the above mentioned scenarios. Therefore, it deserves investigation.

We address these questions using a model system - the early embryonic development of *Drosophila melanogaster*. This system is interesting for several reasons. First of all it is a well studied organism biologically - most genes forming the transcriptional network are identified. Second, the transcriptional network that controls the early development of this organism contains a relatively small number of genes, of the order of ten genes[2] [20]. This makes this organism a particularly appealing model system for studying the properties of transcriptional networks.

---

[2]If we focus on the anterior-posterior patterning.

At the stage that we study the embryo is one giant cell (about half a millimeter long). Unlike most biological cells that have one nucleus per cell, this particular cell has many nuclei. Each nucleus contains its own transcriptional network and produces the messenger RNAs that can be translated into proteins. There are no cellular membranes that separate the nuclei at this stage therefore the proteins can diffuse throughout the embryonic cell. Fig. 1.1 schematically illustrates the structure of the network. We consider the spatial distribution of the proteins inside the cell along the anterior-posterior axis, which is the coordinate along the major axis of the embryo ($x = 0$ corresponds to the position of the head of the future organism, $x = 1$ corresponds to the posterior extreme). There are several morphogens that are deposited inside the cell (the embryo of the fruit fly) in a position-dependent way prior to the stage that we study. These are called the maternal morphogens. The anterior-posterior dependence of one of them - the Bicoid protein - is shown on the left panel. These morphogens serve as an input into the network of downstream genes - the gap genes. Since the inputs are coordinate-dependent, the network of the gap genes operates in different regimes at different positions inside the cell. Thus the crucial role of the maternal inputs is to break the translational invariance inside the cell. As an output from the gap gene network we observe a sophisticated pattern of expression. The mean expression pattern (averaged over the ensemble of many cells) as a function of the anterior-posterior axis is shown on the right panel. The error bars on this graph show the variability of the expression profiles across the ensemble of cells. These fluctuations - deviations of the profile in an individual cell from the mean profile - are the main subject of the present dissertation. As we know from many examples in physics, the structure of correlations of these fluctuations can carry information about the underlying equations (that encode the architecture of the transcriptional network) describing the production of this pattern. More importantly,

6

it can carry information about which particular phase the network is operating in, on the phase diagram of all the networks that one can imagine theoretically.

Before proceeding, we would like to emphasize that although part of our message is that the existing experimental data can be interpreted from the perspective of the criticality hypothesis, this statement is not the main goal of this part of the dissertation. Rather, the main goal is theoretical exploration. What would morphogenesis look like at criticality? How can we describe theoretically the relevant degrees of freedom in such systems? These are examples of the main questions that we will try to address.

Another important issue is that criticality may not be, and does not have to be, exact for the purposes of our discussion. What is important is a sufficiently large separation of scales in the effective mass of the zero mode and of the remaining excitations. If such separation exists, the concept of criticality might provide a theoretical tool for systematic identification of relevant degrees of freedom in the system (and perhaps more generally in biological systems). Importantly, these relevant degrees of freedom will be collective excitations (involving simultaneous variation of all the proteins in the network) and not the physical degrees of freedom (involving the change of one particular protein).

## 1.3   Historical Comments

In this section we will try to put the questions that we discuss in the present dissertation in historical context. We will outline some of the previous ideas and results that has led to or influenced in a significant way the questions discussed in the dissertation. We also discuss some of the subsequent developments.

## De Sitter space

An important landmark in de Sitter physics is the paper [8] by Chernikov and Tagirov and the paper [7] by Bunch and Davies that defined a propagator (known as the Bunch-Davies propagator) as an analytic continuation from the sphere (where the propagator is uniquely defined). For a while this propagator was (incorrectly) interpreted as the Feynman propagator on the de Sitter space. This propagator, however, is real at coincident points, therefore, if interpreted as the Feynman one, one must conclude that there is no particle production in the de Sitter space. This (incorrect) conclusion was adopted for example in the classical textbook [6] as well as in numerous other papers. It contradicts, however, results obtained by the method of Bogolyubov transformations. In the Bogolyubov framework, the reflection coefficients are non-zero, suggesting that particles are being produced. The puzzle was solved (to the best of my knowledge for the first time) in [40], where it was shown that the Bunch-Davis propagator is the in-in propagator and not the Feynman one. The subsequent investigation in [28] (see appendix B) pointed out that the latter statement is true only when we are talking about the Poincare patch and not the complete de Sitter space. Both in-in and in-out propagators for the complete de Sitter space are different from the Bunch-Davies one. Among many other things, the paper [40] suggested the composition principle, which is the criterion for selecting the Feynman propagator among other Green functions.

The existence of infrared divergences resulting from loop corrections was addressed in [28]. It was shown (in the one loop approximation) that the infrared corrections to the Green functions appear both in the Poincare patch as well as in the complete de Sitter space. In the Poincare patch this correction modifies the behavior of the Green function at large distances. Direct resummation of leading logarithms has been done in [22]. Although the technical results of [22] coincide with the results of [28], the interpretation of this correction as an imaginary renormalization of mass

seems problematic. If this were true, then one of the terms in the renormalized version of Eq (2.22) would decay faster compared to the corresponding term in the bare Green function, while the other term would decay slower. This is not what is happening - both terms are decaying faster [28]. Another result of [28] is the existence of infrared corrections in the complete de Sitter space. These corrections have a strong dependence on the infrared cutoff in the past. Explicit resummation of these contributions remains an open problem to the best of my knowledge. As was pointed out in [34], these results are beyond the reach of the Euclidean formalism, and therefore require calculations in the de Sitter space. It was also pointed out in [34] that these corrections disappear in the limit where the argument of the Green function is taken to infinite future. It is not clear to what extent such a problem is physical, however, since to reach this future infinity we will have to pass through the region where this correction was already large at earlier times. Thus, it seems to me that subsequent work is required to clarify these issues.

## Criticality

The idea that biological systems might operate near a critical point or critical surface is not new. There have been a lot of discussions in the past about self-organized criticality [2], criticality tuned by learning mechanisms [33], criticality in boolean networks [23] (see also a recent revitalization of these ideas in [1] ), etc. Although the idea might look quite plausible on a qualitative level, it languished for lack of connection to experiments. It has re-emerged [36] through the analysis of new data on systems with large numbers of elements, such as networks of neurons [45], flocks of birds [4], or the network of interactions among amino acids that determine the structure of proteins in a given family [37]. In these various problems, however, the appearance of criticality looks very different from the point of view of both theoretical description and experimental signatures. In the context of self-organized criticality, the discussion

is centered around the power law in the distribution of sizes of avalanches [2]. In the context of networks of neurons [45] and the diversity of antibodies [37], the signatures of criticality are seen through the lens of the maximum entropy models and Zipf law. In the context of flocks of birds [4] and transcriptional networks [27] the key element is the behavior of the correlation functions. These individual observations may look quite unrelated at the moment, therefore it would be interesting to see if they are different parts of a single general phenomenon.

# Chapter 2

# Infrared effects in external backgrounds

In this chapter we discuss the process of non-equilibrium particle production in external electric and gravitational fields. These backgrounds violate either conservation or positivity of energy, thus allowing creation of particles from vacuum. Because of its non-equilibrium nature these processes can not be described in the conventional language of Feynman diagrams and require a special treatment based on the Schwinger-Keldysh formalism [44, 24]. We discuss the vacuum expectation values of the scalar field in the expanding Poincare patch and in the complete de Sitter space, and show that the infrared corrections appear in both cases. In the case of the Poincare patch these corrections modify the behavior of the Green function at large distances. In the case of the complete de Sitter space these corrections contribute to the interference term of the Green function, and therefore are much stronger. We start with a toy model example of a strong electric field, to illustrate the main features of the formalism that is used in the subsequent sections for the gravitational backgrounds.

The text of this chapter has previously been published in [28].

## 2.1  Infrared dependence of the induced current (free fields)

Pair production by electric fields has been discussed in hundreds of papers. We return to this problem for two reasons. First, we need to present it in a form which can be easily generalized to the gravitational case. Second, we will find an unusual anomalous vacuum polarization which may have unexpected applications.

Let us consider a massive scalar field in an electric field, described by a time-dependent vector potential $A_1(t)$. We assume that the electric field is switched on and off adiabatically. This means that it has the form $E = E(\frac{t}{T})$ so that for $|t| << T$, it remains constant while for $|t| >> T$, $E \rightarrow 0$. A good concrete example of such behavior (already considered in [38]) is to take

$$A_1(t) = ET \tanh\left(\frac{t}{T}\right) \tag{2.1}$$

$E(t) = \frac{E}{\cosh(\frac{t}{T})^2}$, but the explicit shape of the potential is not important. The Klein-Gordon equation has the form

$$\left(\partial_t^2 + \left(k - A(t)\right)^2 + k_\perp^2 + m^2\right)\varphi = 0 \tag{2.2}$$

We are interested in the 'in' solution which is defined as the 'Jost function', i.e. it has the asymptotic behavior

$$\varphi_{in}(t,k) \rightarrow_{t \to -\infty} \frac{1}{\sqrt{2\omega_k^-}} e^{-i\omega_k^- t} \tag{2.3}$$

where $\omega_k^\pm = \sqrt{\left(k - A(\pm\infty)\right)^2 + k_\perp^2 + m^2}$. The solution is normalized by the condition that Wronskian $W(\varphi, \varphi^*) = -i$.

As we go to late times $t \to \infty$, we have

$$\varphi_{in}(t, k) \to_{t \to \infty} \frac{1}{\sqrt{2\omega_k^+}} \left[ \alpha(k) e^{-i\omega_k^+ t} + \beta(k) e^{i\omega_k^+ t} \right] \tag{2.4}$$

where $\alpha$ and $\beta$ are Bogolyubov coefficients also related to the transmission and reflection amplitudes.

If we start with $\varphi_{in}$ and blindly apply the WKB approximation, we get

$$\varphi_{in}(t, k) \sim \frac{1}{\sqrt{2\omega_k(t)}} e^{-i \int_0^t \omega_k(t') dt'} \tag{2.5}$$

for late times, with $\omega_k(t) = \sqrt{(k - A(t))^2 + k_\perp^2 + m^2}$. Of course, this way we lose the over barrier reflection and thus the above formula cannot be valid everywhere. Indeed the WKB requires that the de Broglie wave length $\lambda = \frac{1}{\omega_k}$ satisfies

$$\gamma = \frac{d\lambda}{dt} = \frac{(k - A)\dot{A}(t)}{\left[ (k - A)^2 + k_\perp^2 + m^2 \right]^{\frac{3}{2}}} \ll 1 \tag{2.6}$$

We see that the approximation is good for the early times when $|k - A(t)| \gg m$. In this case

$$\gamma \sim \frac{E}{|k - A|^2} \sim \frac{m^2}{|k - A|^2} \frac{E}{m^2} \ll 1 \tag{2.7}$$

if we assume $E \sim m^2$.

However, around the point where the mode 'reaches the horizon', defined by $k = A(t_k)$, we get $\gamma \sim 1$ and the WKB breaks down. As we go to $t \gg t_k$, $|k - A|$ starts growing again and the WKB is valid again. In this region the solution must contain two exponentials:

$$\varphi_{in}(t, k) \sim \frac{1}{\sqrt{2\omega_k(t)}} \left[ \alpha(k) e^{-i \int_0^t \omega_k(t') dt'} + \beta(k) e^{i \int_0^t \omega_k(t') dt'} \right] \qquad t \gg t_k \tag{2.8}$$

As usual, $\alpha$ and $\beta$ can be found by matching (2.3) and (2.8).

In the domain $|t| \ll T$ the electric field is constant and $A(t) \sim Et$. The equation (2.2) now depends on the variable $t - \frac{k}{E}$, hence $\varphi_{in} \sim f_{in}(t - \frac{k}{E})$. The function $f_{in}$, as well known, is the parabolic cylinder function

$$\varphi_{in} \sim D_{-\frac{1}{2} - i\lambda}\left[ -\sqrt{2E}e^{i\frac{\pi}{4}}(t - \frac{k}{E})\right] \qquad t \to -\infty, \qquad \lambda = \frac{m^2 + k_\perp^2}{2E} \qquad (2.9)$$

but we will not need its explicit form. What is important is that due to the symmetry $k \to k + \kappa$, $t \to t - \frac{\kappa}{E}$ the resulting $\alpha$ and $\beta$ do not depend on $k$ in a certain range, which we determine in a moment, but do depend on $k_\perp$ and $m$.

To find this range we notice that the 'horizon crossing' $(k = A(t))$ occurs at $t_k = \frac{k}{E}$. We can use the constant field approximation only if $t_k \ll T$. Hence we conclude that $\alpha$ and $\beta$ do not depend on $k$ only if $A(-\infty) < k < A(\infty)$. Outside this interval, the reflection coefficient $\beta$ quickly decreases to zero.

The field $\varphi$ can be expanded in terms of creation and annihilation operators as

$$\varphi = \sum_k \left( a_k f_k^{in*} e^{ikx} + b_k^\dagger f_k^{in} e^{-ikx} \right) \qquad (2.10)$$

and the Green function is equal to

$$G(x_1, t_1 | x_2, t_2) = {}_{in}\langle 0|T\varphi(x_1, t_1)\varphi(x_2, t_2)^*|0\rangle_{in} = \int f_k^{in}(t_<) f_k^{in*}(t_>) e^{ik(x_1 - x_2)} dk$$

$$(2.11)$$

We can calculate the induced current which can be used to estimate the back reaction. The general formula for the current is

$$\langle J(t)\rangle = \int \left(k - A(t)\right)|\varphi_{in}(k, t)|^2 \, dk$$

As we will see, the current is dominated by the two semi-classical domains described above. Before the 'horizon crossing' we have

$$\langle J(t)\rangle^{(1)} = \int\limits_{A(t)<k} dk\ dk_\perp \frac{(k-A(t))}{2\omega_k(t)} = \int\limits_0^\infty \frac{dp\ p\ dk_\perp}{2\sqrt{p^2 + k_\perp^2 + m^2}} \qquad (2.12)$$

where $p = k - A(t)$ is 'physical momentum'. After horizon crossing, we have to use (2.4). Keeping only non-oscillating terms, which are dominant, we obtain

$$\langle J\rangle^{(2)} = \int\limits_{k<A(t)} dk\ dk_\perp \frac{k-A(t)}{2\sqrt{(k-A)^2 + k_\perp^2 + m^2}}\left(|\alpha(k)|^2 + |\beta(k)|^2\right)$$

Using the general relation $|\alpha(k)|^2 - |\beta(k)|^2 = 1$ we get:

$$\langle J\rangle^{(2)} = \int\limits_{-\infty}^0 \frac{dp\ dk_\perp\ p}{2\sqrt{p^2 + k_\perp^2 + m^2}} + 2\int\limits_{-\infty}^0 \frac{dp\ dk_\perp\ |\beta(k,k_\perp)|^2\ p}{2\sqrt{p^2 + k_\perp^2 + m^2}}$$

The first term in this formula combines with (2.12) and gives zero due to $p \to -p$ symmetry. The second term is really interesting. The key feature of it is that the reflection coefficient $\beta$ depends on the 'comoving' momentum $k$ and not the physical one $p$. As we saw, this coefficient is constant for $A(-\infty) \ll k \ll A(\infty)$ and quickly vanishes outside this interval. In terms of $p$, this means the time-dependent cut-off $A(-\infty) \ll p + A(t) \ll A(\infty)$. We also have a cut-off on $k_\perp$, $k_\perp \ll E^{1/2}$. Hence, the total current is given by

$$\langle J\rangle = \int\limits_{A(-\infty)-A(t)}^0 dp\ \frac{p}{|p|}\int dk_\perp\ |\beta(k_\perp,k)|^2 = -\Big(A(t) - A(-\infty)\Big)|\beta|^2 E^{\frac{d-1}{2}} \cdot const \quad (2.13)$$

In the last expression $|\beta|^2 = e^{-\frac{\pi m^2}{E}}$. This result is physically transparent. It means that, as time goes by, more and more $k$ modes cross the horizon $k = A(t)$ and begin to contribute to the induced current. This fact is important. It shows

15

that the induced current is proportional to the vector potential and not the field strength. Together with gauge invariance this implies a highly non-local behavior. Indeed, $A(t) - A(-\infty) = \int_{-\infty}^{t} dt' E(t')$. Thus, the gauge invariant expressions can't be expressed locally in terms of the field strengths.

This result implies a strong back reaction, since the current is growing with time. Another interpretation of this result is symmetry breaking. Indeed, in the constant field we have time translation invariance. This invariance is broken in the expression for the current due to the influence of the past when the field was turning on. We will return to this phenomenon later, while discussing the gravitational case.

We can also use the in/out Green function

$$G^{in/out} = \frac{1}{\alpha} \varphi_k^{in}(t_<) \varphi_k^{out*}(t_>)$$

The sign of vacuum instability here is $ImG(t|t) \neq 0$. Let us notice that the matrix element $\langle out|J_1|in \rangle = 0$ because the in/out Green function is Lorentz invariant (modulo a phase factor).

It is also instructive to change the gauge. If we take $A_0 = Ez$ we get the Klein-Gordon equation

$$(\partial_z^2 + (\omega - Ez)^2 - m^2)\varphi = 0$$

As in the time-dependent gauge, we have a Schrodinger equation for an inverted oscillator, but this time the effect of pair creation comes from the underbarrier penetration rather than from the overbarrier reflection. The two are related by the analytic continuation. In this gauge the energy $\omega = Ez + \sqrt{p^2 + m^2}$ is conserved but non-positive which allows particle production.

## 2.2 Expanding Universe (free fields)

When we look at the de Sitter space, we find that there are striking similarities with the electric case. Let us consider what happens when the curvature of $dS$ space is adiabatically switched on. In this setting we have two quite different problems - expanding and contracting universes. The arrow of time is set up by defining the infinite past as a Minkowski space in which our field is in the ground state and solutions to the wave equation are chosen to be the Jost functions. Let us begin with the expanding Universe. Analogously to the electric case we will assume that the FRW metric

$$ds^2 = a(t)^2 d\vec{x}^2 - dt^2$$

is such that $\frac{\dot{a}}{a} = H(\frac{t}{T})$, time $T$ is supposed to be large, and $H(0) = 1$, while $H(\pm\infty) = 0$. A representative example of such a metric is

$$a(t) = e^{T\tanh\frac{t}{T}}$$

$H(t) = \frac{1}{\cosh(\frac{t}{T})^2}$. It is convenient to rescale the standard scalar field $\varphi$ by defining $\varphi = a^{-\frac{d}{2}}\phi$. The Klein-Gordon equation takes the form

$$\ddot{\phi}_{in} + \left(m^2 - r(t) + \frac{k^2}{a(t)^2}\right)\phi_{in} = 0$$

with $r(t) = \frac{d(d-2)}{4}(\frac{\dot{a}}{a})^2 + \frac{d}{2}\frac{\ddot{a}}{a}$. As before, the 'in' solution is defined by

$$\phi_{in} = \frac{1}{\sqrt{2\omega_k^-}}e^{-i\omega_k^- t} \tag{2.14}$$

as $t \to -\infty$ with $\omega_k^- = \left(m^2 + \frac{k^2}{a(-\infty)^2}\right)$. Its quasiclassical expression is given by the formula (2.5) where $\omega_k(t) = \sqrt{m^2 - r(t) + \frac{k^2}{a(t)^2}}$. This WKB expression is applicable

if

$$\gamma \; = \; \dot{\lambda} \; = \; \frac{d}{dt}\left(\frac{1}{\omega_k}\right) \; \sim \; \frac{1}{\left(m^2 - r + \frac{k^2}{a^2}\right)^{\frac{3}{2}}} \frac{k^2}{a^2}\frac{\dot{a}}{a} \; \ll \; 1$$

If we assume that $H = \frac{\dot{a}}{a} \sim m$ and $\dot{H}$ is small, we see that WKB breaks down when the given mode crosses the horizon, $k \sim ma(t)$. Before that we had $k \gg ma(t)$ and $\dot{\lambda} \ll 1$. Long after that, we reach the semi-classical regime again, but with two exponentials as in (2.4). Let us consider the time evolution of the quantity $\langle in|\varphi(t)^2|in\rangle$. We have:

$$\langle in|\varphi(t)^2|in\rangle \; = \; \int d^d k \; |\varphi_{in}(t,k)|^2$$

Splitting the integral as before into the regions $|k| \gg ma(t)$ and $|k| \ll ma(t)$ we get

$$
\begin{aligned}
\langle in|\varphi(t)^2|in\rangle \; = \; & a(t)^{-d} \int\limits_{|k|\gg ma(t)} \frac{d^d k}{2\omega_k(t)} \; + \; a(t)^{-d} \int\limits_{|k|\ll ma(t)} \frac{d^d k}{2\omega_k(t)}\left[|\alpha(k)|^2 + |\beta(k)|^2\right] \; = \\
= \; & a^{-d}\left(\int \frac{d^d k}{2\omega_k(t)} \; + \; 2 \int\limits_{|k|\ll ma(t)} \frac{d^d k}{2\omega_k(t)}|\beta(k)|^2\right)
\end{aligned}
$$

$$(2.15)$$

The reflection amplitude $\beta(k)$ is $k$-independent in a certain interval, just as it was in the electric case. The reason is that the de Sitter wave equation is invariant under $k \to \lambda k$ and $t \to t + \log \lambda$. However this amplitude quickly vanishes when $k$ is such that the horizon crossing happens outside the de Sitter stage. Namely, if $t_k$ is determined from the equation $k = ma(t_k)$, the constant reflection occurs for $|t_k| \ll T$. If we introduce the cut-offs defined by $\frac{k_{min}}{a(-\infty)} = k_{min}e^T = m$ and $\frac{k_{max}}{a(+\infty)} = k_{max}e^{-T} = m$, we have reflection only if $k_{min} \ll k \ll k_{max}$. We see that the contribution of the second term in (2.15), which represents the created particles, is small in the expanding case.

Due to the infrared convergence of the integral we obtain

$$\langle \varphi(t)^2 \rangle^{(2)} \ \sim \ |\beta|^2 m^{d-1} \tag{2.16}$$

This formula has a clear physical interpretation. By the moment $t$ we excite the modes with $|k| < ma(t)$ and the average excitation number is $\overline{n} \sim |\beta|^2$. The created particles are non-relativistic due to the upper boundary on $k$. Let us stress that there is no dilution of the created particles in the sense that their physical (not comoving) density remains constant in time, however their main contribution is just a renormalization of the cosmological constant which is unobservable.

The key difference from the electric case is the absence of dynamical symmetry breaking, which we define as a long-term memory. By this we mean the following. As we already noted, the current in the electric case depends on the time passed from the first appearance of the field. This effect is a dynamical counterpart of the usual spontaneous symmetry breaking. In the latter case, the magnetic field at the boundary induces magnetic moment in the bulk, as in the Ising model for example. In our case the role of the boundary is played by the infinite past. The expression (2.16) does not depend on time. Hence, there is no dynamical breaking of de Sitter symmetry in this case. Life becomes more interesting if we switch on interactions or consider a contracting universe.

We could calculate things in the regime of the constant curvature and get the right results. In this case

$$\varphi_{in} \ \sim \ \tau^{\frac{d}{2}} H_{i\mu}^{(1)}(k\tau)$$

with $\tau = e^{-t}$ and

$$\langle in|\varphi(t)^2|in \rangle \ \sim \ \tau^d \int d^d k \ |H_{i\mu}^{(1)}(k\tau)|^2 \ = \ \int d^d p \ |H_{i\mu}^{(1)}(p)|^2 \ = \ const$$

The UV divergence in this integral is the same as in the flat space and the time independence in this formula is just the result of the de Sitter symmetry. The back reaction is thus small and uninteresting. Really non-trivial things begin to happen when we either include interactions or consider a contracting universe. We start with the latter.

## 2.3 Contracting Universe (free fields)

Let us repeat the above calculations in the case of the contracting Universe. At the first glance it may seem that, since the de Sitter space is time-symmetric, expansion and contraction can't lead to different results. However, as was stated above there is an arrow of time in our problem. We defined the past by the condition that our field is in the Minkowski vacuum state. Generally speaking, in the future we should expect a complicated excited state. In this setting contraction is very different from expansion. We can once again take

$$a(t) = e^{-T \tanh \frac{t}{T}}$$

The modes with $k > ma(-\infty) = me^T$ will always stay in the WKB regime, since $a(t)$ will be decreasing. On the other hand, the modes with $ma(\infty) \ll k \ll ma(-\infty)$ will cross the horizon at some time, $k \approx ma(t_k)$. If we once again define the 'in' modes, $\varphi_{in}(k,t)$ by the condition (2.14), we find that for $k \ll ma(t)$ the horizon crossing (WKB breaking) has not occurred yet (remember that $a(t)$ is decreasing) and hence we have a single exponential (2.14).

For $ma(t) \ll k \ll ma(-\infty)$ the horizon crossing is already in the past and we have two exponentials with coefficients $\alpha$ and $\beta$, which satisfy $|\alpha(k)|^2 - |\beta(k)|^2 = 1$. For $k \gg ma(-\infty)$, the horizon crossing has never occurred and $\beta \to 0$. As in the

20

previous section we get

$$\langle in|\varphi(t)^2|in\rangle = a(t)^{-d} \int\limits_{|k|\ll ma(t),\ |k|\gg ma(-\infty)} \frac{d^d k}{2\omega_k(t)} + a(t)^{-d} \int\limits_{ma(t)\ll|k|\ll ma(-\infty)} \frac{d^d k}{2\omega_k(t)}\left[|\alpha(k)|^2 + |\beta(k)|^2\right] =$$

$$= a^{-d}\left(\int \frac{d^d k}{2\omega_k(t)} + 2\int\limits_{ma(t)\ll|k|\ll ma(-\infty)} \frac{d^d k}{2\omega_k(t)}|\beta(k)|^2\right)$$

(2.17)

Collecting different terms we get

$$\langle\varphi(t)^2\rangle = a^{-d} \int\limits_{|k|\ll\Lambda a(t)} \frac{d^d k}{2\omega_k} + 2|\beta|^2 a^{-d} \int\limits_{ma(t)<|k|<ma(-\infty)} \frac{d^d k}{2\omega_k(t)} \approx$$

(2.18)

$$\approx const\cdot\Lambda^{d-1} + |\beta|^2\left(\frac{a(-\infty)}{a(t)}\right)^{d-1} m^{d-1}$$

The first term in this formula is just the same UV divergent term as in the Minkowski space. The heart of the matter is the second term which displays the symmetry breaking through the long-term memory (dependence on $a(-\infty)$). However, the memory can't be too long, since we have a standard UV cut-off at the Planck mass. Because of this, the above formulae are valid if $p = k/a(t) < M_{pl}$ and therefore $a(-\infty)/a(t) < M_{pl}/m$.

Let us sum up the above discussion. In the expanding universe the contribution from the created particles comes from the region $ma(-\infty) \ll k \ll ma(t)$. No long term memory is present, and the time-dependent back reaction is small, of the order of $\left(\frac{a(-\infty)}{a(t)}\right)^{d-1}$. Created particles are non-relativistic due to the red shift.

In the case of the contracting universe, particles come from $ma(t) < |k| < \min\left(ma(-\infty),\ M_{pl}a(t)\right)$. They are ultra-relativistic and their contribution is of the order $\left(\frac{a(-\infty)}{a(t)}\right)^{d-1} \to \infty$. All these conclusions are correct only for non-interacting particles.

It is also possible to calculate the energy-momentum tensor. We have

$$
T_{00} = \int d^d k \left( (\partial_0 \varphi)^2 + \frac{1}{a(t)^2}(\partial_i \varphi)^2 + m^2 \varphi^2 \right)
$$

In the contracting case the order of magnitude of this quantity is defined by the integral:

$$
T_{00} \sim a^{-d} \int \frac{d^d k}{2\omega_k} \frac{k^2}{a^2} \, |\beta|^2 \sim a^{-d-1} \int_{ma<k<ma(-\infty)} d^d k \, |k| \, |\beta|^2 \sim m^{d+1} \left( \frac{a(-\infty)}{a(t)} \right)^{d+1} |\beta|^2
$$

This corresponds to ultra-relativistic particles with the equation of state $p = \frac{1}{d}\varepsilon$. In the expanding case the contribution to $T_{00}$ comes from a small number of created non-relativistic particles. In both cases there is no reason to believe that created particles are in thermal equilibrium. Let us also stress that the above formula represents a non-local contribution to $T_{00}$ similar to (2.13). In contrast with this formula, the local contributions should depend on the quantities taken at the time $t$ only.

## 2.4 Secular interactions and the leading logarithms, Poincare patch

In this section we discuss a very peculiar property of the de Sitter space. Namely, it turns out that the interactions of massive particles generate infrared corrections. We start with the second order of perturbation theory in the case of $\lambda \varphi^3$ interactions (which we choose to simplify notations; the phenomenon we are after is general and has nothing to do with the naive lack of the ground state of the above interaction). We first calculate the correction to the Green's function $G(\vec{q}, \tau) = \langle in|\varphi(\vec{q}, \tau)\varphi(-\vec{q}, \tau)|in\rangle$ where $\vec{q}$ is a comoving momentum in the Poincare patch and $\tau$ is a conformal time. Our goal is to show that if the physical momentum $p = q\tau \ll \mu$, there are corrections

of the order $(\lambda^2 \log \frac{\mu}{p})^n$ where $\mu$ is the particle mass; notice also that these logarithms are powers of the physical time $t = -\log \tau$.

We are interested in the loop corrections to the one-point function $\langle \varphi(t)^2 \rangle$. The magnitude of this quantity determines the strength of the backreaction. To find it we have to use the Schwinger- Keldysh perturbation theory. These methods are well known and we will add a few explanations to specify notations. Let us suppress first the momentum dependence and expand $\varphi = f^*a + fa^+$ , where $f(t)$ are the "in" modes and $a$ is the annihilation operator. The relevant one-loop diagram is shown at Fig.3. Its contribution to $G(\vec{q}, \tau) = \langle in| \varphi(\vec{q}, \tau) \varphi(-\vec{q}, \tau) |in \rangle$ is given by

$$
G(\vec{q}, \tau) = -\lambda^2 f_q^*(t)^2 \int\limits_{-\infty}^{t} dt_1 dt_2 \, f_q(t_1) f_q(t_2) \int \frac{d^d k}{(2\pi)^d} \, f_k(t_<) f_k^*(t_>) f_{k+q}(t_<) f_{k+q}^*(t_>)
$$

$$
-c.c. \, + \, 2 \cdot \lambda^2 \, |f_q(t)|^2 \int\limits_{-\infty}^{t} dt_1 dt_2 \, f_q(t_1) f_q^*(t_2) \int \frac{d^d k}{(2\pi)^d} \, f_k(t_1) f_k^*(t_2) f_{k+q}(t_1) f_{k+q}^*(t_2)
$$

$$(2.19)$$

In the first line we have the contribution of the $(+/+)$ and $(-/-)$ diagrams (the signs refer to the points $t_{1,2}$ of the physical time, or $\tau_{1,2}$ of conformal time at the diagram in Fig.3), while in the second line we have $(+/-)$ and $(-/+)$ diagrams.
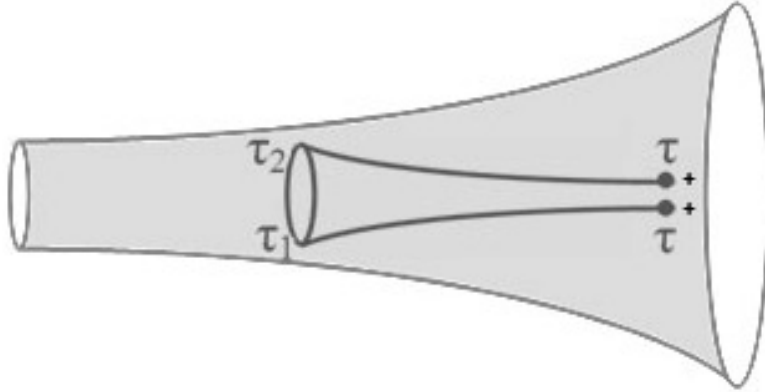


Figure 2.1: One-loop diagram responsible for infrared logarithms in Poincare patch.

We choose the "in" wave function to be the Hankel function

$$f_k(t) = \tau^{\frac{d}{2}} h(k\tau) = const\ \tau^{d/2} H^{(1)}_{i\mu}(k\tau)$$

where the normalization is fixed by the condition $h(x) \to (2x)^{-\frac{1}{2}} e^{ix}$ as $x \to \infty$. With this normalization, the asymptotic behavior at $x \to 0$ is given by

$$h(x) \to A(\mu) x^{i\mu} + A(-\mu) x^{-i\mu} \qquad (2.20)$$

where $A$-s are some specific functions which we discuss later.

As we will show in a moment, there are infrared logarithmic corrections to $G(\vec{q}, \tau) = \tau^d g(q\tau)$ when $q\tau \ll \mu$. In this regime we can use asymptotic expressions (2.20) to get, $\tilde{\lambda} = \lambda^2 \log\left(\frac{\mu}{q\tau}\right)$

$$g(x) = A(\mu) A^*(-\mu)\, \Gamma(\tilde{\lambda}, \mu)\, x^{2i\mu} + A(-\mu) A^*(\mu)\, \Gamma^*(\tilde{\lambda}, \mu)\, x^{-2i\mu} + \left(|A(\mu)|^2 + |A(-\mu)|^2\right) C(\tilde{\lambda}, \mu)$$

when the interaction is off ($\tilde{\lambda} = 0$), the coefficients $\Gamma^{(0)} = C^{(0)} = 1$. Our goal is to find these quantities at non-zero $\lambda$. We start with the interference term $C$.

In order to obtain the contribution to $g(q\tau)$ we have to integrate the diagrams of Fig.3 over the momentum $k$ and the time variables $t_1$ and $t_2$ . The logarithmic contribution comes from the domain $\tau_{1,2} \sim \mu/k$ and $\mu/\tau \gg k \gg q$. In this domain we get the contribution from the first term in (2.19) in the form

$$g(q\tau)_I = -2\lambda^2\, h^*(q\tau)^2 \int d^d k \int_\tau^\infty d\tau_1 \int_{\tau_1}^\infty d\tau_2 (\tau_1 \tau_2)^{d/2-1} h(q\tau_1) h(q\tau_2) h^*(k\tau_1)^2 h(k\tau_2)^2 - c.c.$$

Taking the limit $q \to 0$ and interchanging 1 and 2 in the complex conjugate term gives

$$g(q\tau)_I = \int_q^{\frac{\mu}{\tau}} \frac{d^d k}{k^d} C_I(\mu) = C_I \log(\frac{\mu}{q\tau})$$

24

Here the coefficient is given by

$$
\begin{aligned}
C_I &= -4\lambda^2 |A(\mu)A(-\mu)|^2 (|g(\mu)|^2 + |g(-\mu)|^2) \\
g(\mu) &= \int_0^\infty dx \, x^{d/2-1+i\mu} \, h^2(x)
\end{aligned}
$$

The second term is treated analogously. It has the form

$$
g(q\tau)_{II} = 2\lambda^2 h^*(q\tau)h(q\tau) \int d^d k \int_\tau^\infty d\tau_1 d\tau_2 (\tau_1\tau_2)^{d/2-1} h^*(q\tau_1)h(q\tau_2)h^*(k\tau_1)^2 h(k\tau_2)^2
$$

$$(2.21)$$

Integration gives another logarithm. Summing these contributions finally gives us the interference term

$$
\langle \varphi_q^2 \rangle = g(q\tau)_I + g(q\tau)_{II} = 2 \cdot \Big( B(\mu) - B(-\mu) \Big) \cdot \Big( B(\mu)|g(\mu)|^2 - B(-\mu)|g(-\mu)|^2 \Big) \cdot \lambda^2 \log\left(\frac{\mu}{q\tau}\right)
$$

where

$$
B(\mu) = |A(\mu)|^2 = \frac{1}{4\mu} e^{\pi\mu} \frac{1}{\sinh(\pi\mu)}
$$

The first multiple here is a Wronskian of the eigenmodes. The second one turns out to be equal to zero. To see this, note that the functions $h(x)$ satisfy $h(x)^* = e^{i\frac{\pi}{2}} h(e^{i\pi}x)$ which implies the following relation for $g(\mu)$:

$$
|g(\mu)|^2 = e^{-2\pi\mu}|g(-\mu)|^2
$$

The physical meaning of this equality is the detailed balance relation with the Gibbons-Hawking temperature for de Sitter space. Combining this with the similar property for $A(\mu)$, we conclude that the one-loop contribution to the coefficient in front of the logarithmic divergence in the interference term is equal to zero $C^{(1)}(\tilde\lambda, \mu) = 0$.

The next step is to calculate $\Gamma$. The imaginary part of this quantity determines a renormalization of mass $\mu$, which we are not interested in at the moment. Using similar tricks[1] to those used above we find the following expression for the real part

$$Re\left(\Gamma^{(1)}\right) \;=\; \lambda^2\Big(B(\mu) - B(-\mu)\Big)\Big(|g(\mu)|^2 - |g(-\mu)|^2\Big)\log\left(\frac{\mu}{q\tau}\right)$$

This quantity is non-zero and negative.

The above calculation refers to the IR properties of the two-point function. In the case of the Poincare patch there is no IR contribution to the one-point quantities, as can be seen from the conformal diagram in Fig.4. The Poincare patch is shown here by the gray area. Interactions contributing to the one-point function must be located inside the past light cone due to causality. Therefore we have to consider only the intersection of the light-cone with the gray area defining the Poincare patch. Thus
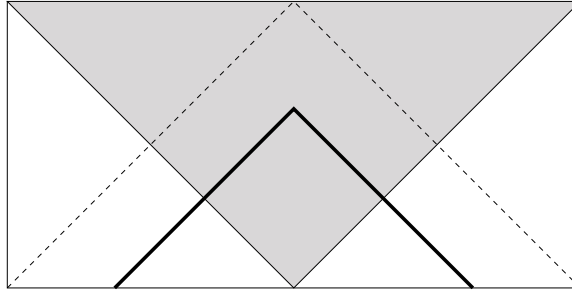


Figure 2.2: Conformal diagram. Poincare patch is shown by the gray area. Solid black line represents the past light cone of the observer. The intersection of this cone with Poincare patch touches past infinity only at one point.

infrared effects in the Poincare patch can not have dramatic consequences because the past infinity is represented only by one point. In the complete de Sitter space the situation is quite different and is discussed in the next section.

---

[1]It is convenient to rescale $k$ from the integrals over $\tau_{1,2}$ and note that

$$Y \;=\; \int\limits_{0}^{\infty} dx \int\limits_{x}^{\infty} dy \; (xy)^{\frac{d}{2}-1}\left(\left(\frac{x}{y}\right)^{i\mu} + \left(\frac{x}{y}\right)^{-i\mu}\right)h(y)^2 h^*(x)^2 \;=\; \frac{1}{2}\left(|g(\mu)|^2 + |g(-\mu)|^2\right) \;+\; iA$$

where $A$ is some real number, contributing to renormalization of $\mu$ only.

26

Although infrared corrections do not appear in the 1-point function $\langle \varphi(t)^2 \rangle$, they contribute to the two point function $\langle \varphi(1)\varphi(2) \rangle$. To illustrate this consider the limit when $\tau_1 = \tau_2 = \tau$ and $x^2 = (\vec{x}_1 - \vec{x}_2)^2 \gg \tau^2$. This corresponds to $z \to -\infty$. The bare Green's function in this limit is given by

$$G_0(z, \mu) \;=\; \frac{1}{\sqrt{-2z}} \Big[ N(\mu)(-z)^{i\mu} \;+\; N(-\mu)(-z)^{-i\mu} \Big] \tag{2.22}$$

The exact Green's function is equal to[2]

$$G(z) \;=\; \Big[ 1 \;+\; \frac{\lambda^2}{2} \Big( B(\mu) - B(-\mu) \Big) \Big( |g(\mu)|^2 \;-\; |g(-\mu)|^2 \Big) \log(-z) \Big] \, G_0(z, \mu + \delta\mu) \;=\;$$
$$=\; \Big[ 1 \;-\; \frac{\lambda^2}{4\mu}(1 - e^{-2\pi\mu})|g(-\mu)|^2 \log(-z) \Big] \, G_0(z, \mu + \delta\mu)$$

We see that besides the infrared renormalization of mass, which we ignore in the present thesis, the bare Green's function is multiplied by the function of $\log(-z)$. Thus, even in the Poincare patch, infrared corrections appear when the two points are separated by a large geodesic distance. It would be interesting to understand the consequences of this result for the inflationary models in the Poincare patch.

## 2.5   Secular interactions and leading logarithms, complete $dS$ space

In order to describe the global $dS$ space, we use the standard metric $ds^2 = dt^2 - \cosh^2 t (d\Omega_d)^2$. The eigenmodes for the Bunch-Davies vacuum are inherited from the

---

[2]To derive this formula we can make a Fourier transform

$$\int^{\frac{\mu}{\tau}} dq \cdot \tau \Big[ A(\mu)A^*(-\mu) \, \Gamma \, (q\tau)^{2i\mu} \;+\; A(-\mu)A^*(\mu) \, \Gamma^* \, (q\tau)^{-2i\mu} \;+\; \big( |A(\mu)|^2 + |A(-\mu)|^2 \big) \, C \Big] \, e^{iqx}$$

and retain only terms of the order $\lambda^2 \log(-z)$ while neglecting the terms of the order $\lambda^2$.

sphere. To simplify notations we write them for $d = 1$:

$$f_q(t) \propto P^{-q}_{-\frac{1}{2}+i\mu}(i \sinh t)$$

where $q$ is an integer. These modes are selected by the condition that they are regular when continued to the southern hemisphere $(t = -i\vartheta;\ \vartheta > 0)$.

The logarithmic divergences appear when $|q| \gg 1$ and $|t| \to \infty$. In this regions the Legendre functions can be replaced by the Bessel functions. We have:

$$f_q(t) \xrightarrow[q \to \infty]{} \begin{cases} \tau^{d/2} h(q\tau), & \tau = e^{-t}, \quad t \to \infty; \\ \\ \widetilde{\tau}^{d/2} h^*(q\widetilde{\tau}), & \widetilde{\tau} = e^{+t}, \quad t \to -\infty. \end{cases}$$

As it should be, this is exactly the doubled Poincare patch.

Let us use these modes to calculate perturbative corrections to $\langle \varphi^2(n) \rangle$, assuming that the interaction begins adiabatically in the far past, with $\widetilde{\tau} = \varepsilon \to 0$, while the "observer" sits in the future at fixed $\tau$. The most important contribution comes from the $+-$ term in the Fig.5. We have
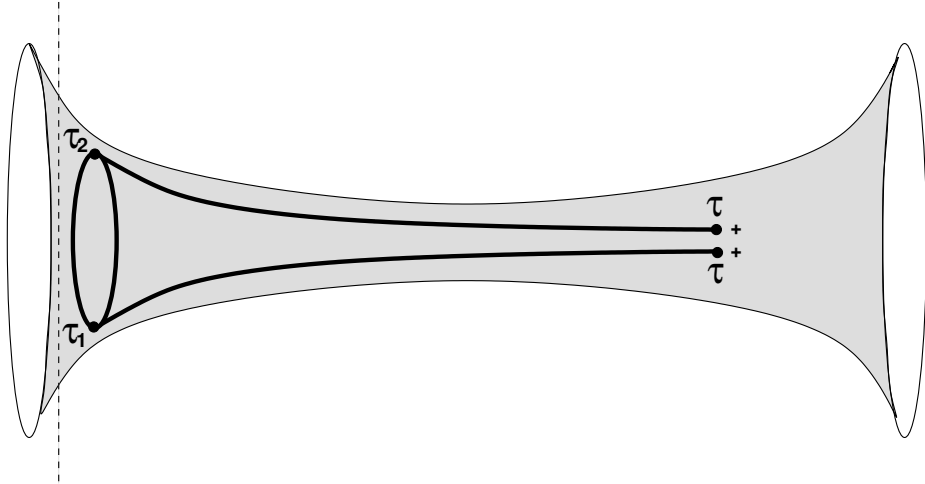


Figure 2.3: Relevant diagram, leading to IR divergence, in complete $dS$ space.

$$\langle \varphi^2(z) \rangle = \lambda^2 \tau^d \int \frac{d^d q}{(2\pi)^d} |h(q\tau)|^2 \int_\varepsilon^\infty \frac{d\widetilde{\tau}_1 d\widetilde{\tau}_2}{\widetilde{\tau}_1 \widetilde{\tau}_2} \left( h^*(q\widetilde{\tau}_1) h(q\widetilde{\tau}_2) \right) \cdot (\widetilde{\tau}_1 \widetilde{\tau}_2)^{\frac{d}{2}} \cdot \sigma_q(\widetilde{\tau}_1, \widetilde{\tau}_2) \quad (2.23)$$

where

$$\sigma_q(\widetilde{\tau}_1, \widetilde{\tau}_2) = \int \frac{d^d k}{(2\pi)^d} h^*(k\widetilde{\tau}_1) h(k\widetilde{\tau}_2) \cdot h^*(|k-q|\widetilde{\tau}_1) h(|k-q|\widetilde{\tau}_2).$$

We consider here only the dominant contribution, when $t_1$, $t_2$ are both in the far past. If $k \gg q$, we get the following property: $\sigma_q(\widetilde{\tau}_1, \widetilde{\tau}_2) \approx \sigma_0(\widetilde{\tau}_1, \widetilde{\tau}_2)$. The integral (2.23) becomes:

$$\langle \varphi^2(z) \rangle = \lambda^2 \tau^d \int \frac{d^d q}{(2\pi)^d} |h(q\tau)|^2 \int \frac{d^d k}{k^d} \int_{k\varepsilon}^\infty dx\, dy \, (xy)^{\frac{d}{2}-1} h^*\left(\frac{q}{k}x\right) h\left(\frac{q}{k}y\right) h^*(x)^2 h(y)^2 =$$

$$= const \cdot \lambda^2 \cdot \tau^d \int d^d q |h(q\tau)|^2 \log\left(\frac{\mu}{q\varepsilon}\right).$$

The UV divergence at large $q$ must be cut off by the condition $q\tau \lesssim M_{pl}$. Thus we get the result

$$\langle \varphi^2(z) \rangle = const \cdot \lambda^2 M_{Pl}^{d-1} \log\left(\frac{\mu}{M_{Pl}} \frac{\tau}{\varepsilon}\right). \quad (2.24)$$

This formula is valid if:

$$\varepsilon \ll \frac{\mu}{M_{Pl}} \tau$$

which means that the time $T$ during which the interaction was on, satisfies

$$T = \frac{1}{H} \log\left(\frac{\tau}{\varepsilon}\right) \gg \frac{1}{H} \log\left(\frac{M_{Pl}}{m}\right)$$

(where we reinstated the Hubble constant).

In the Schwinger - Keldysh language we accounted for the $(+/-)$ self-energy part. There are, of course other insertions, $(+/+)$ and $(-/-)$, also generating secular logarithms. However, they are proportional to $\int d^d q\, h^2(q\tau)$ and its conjugate. This integral is UV convergent due to the oscillations of $h(q\tau)$. Hence there are no UV/IR

mixing in these terms, and their secular contribution, while non-zero, does not contain $M_{pl}$, unlike (2.24).

In higher orders there are higher powers of the logarithms. Their summation requires a renormalization group equation and remains an interesting open problem.

# Chapter 3

# Morphogenesis at criticality? Theoretical signatures and hints from the data

Spatial patterns in the early fruit fly embryo emerge from a network of interactions among transcription factors, the gap genes, driven by maternal inputs. Such networks can exhibit many qualitatively different behaviors, separated by critical surfaces. At criticality, we should observe strong correlations in the fluctuations of different genes around their mean expression levels, a slowing of the dynamics along some but not all directions in the space of possible expression levels, correlations of expression fluctuations over long distances in the embryo, and departures from a Gaussian distribution of these fluctuations. Analysis of recent experiments on the gap genes shows that all these signatures are observed, and that the different signatures are related in ways predicted by theory. While there might be other explanations for these individual phenomena, the confluence of evidence suggests that this genetic network is tuned to criticality.

The text of this chapter has previously been published in [27].

## 3.1 Introduction

Genetic regulatory networks are described by many parameters: the rate constants for binding and unbinding of transcription factors to their target sites along the genome, the interactions between these binding events and the rate of transcription, the lifetimes of mRNA and protein molecules, and more. Even with just two genes, each encoding a transcription factor that represses the other, changing parameters allows for several qualitatively different behaviors [16]. With delays (e.g., in translation from mRNA to protein), mutual repression can lead to persistent oscillations. Alternatively, if mutual repression is sufficiently strong, the two genes can form a bistable switch, admitting both on/off and off/on states, with the choice between these states modulated by inputs to the network [13]. Finally, if interactions are weak, the two interacting genes have just one stable state, and the expression levels in this state are controlled primarily by the inputs. The bistable switch and the graded response to inputs are limiting cases; presumably the real system lies somewhere in between. But if we imagine smooth changes in the strength of the repressive interactions, the transition from graded response to switch–like behavior is *not* smooth: the behavior is qualitatively different depending on whether the relevant interactions are stronger or weaker than a critical value. Here we explore the possibility that the gap gene network in the *Drosophila* embryo might be tuned to such a critical point.

Early events in the fruit fly embryo provide an experimentally accessible example of many questions about genetic networks [39, 29, 15]. Along the anterior–posterior axis, for example, information about the position of nuclei flows from primary maternal morophogens to the gap genes, shown in Fig 3.1 [20, 11, 12], to the pair rule and segment polarity genes. Although the structure of the gap gene network is not completely known, there is considerable evidence that the transcription factors encoded by these genes are mutually repressive [20, 19, 47, 18]. If we focus on a small region near the midpoint of the embryo (near $x/L = 0.47$), then just two gap genes, *hunch-*

*back* (Hb) and *krüppel* (Kr), are expressed at significant levels, and this is repeated at a succession of crossing points or expression boundaries: Hb–Kr, Kr–Kni (*knirps*; $x/L = 0.57$), Kni–Gt (*giant*; $x/L = 0.66$), and Gt–Hb ($x/L = 0.75$), as we move from anterior to posterior. In each crossing region, it is plausible that the dynamics of the network are dominated by the interactions among just the pair of genes whose expression levels are crossing.
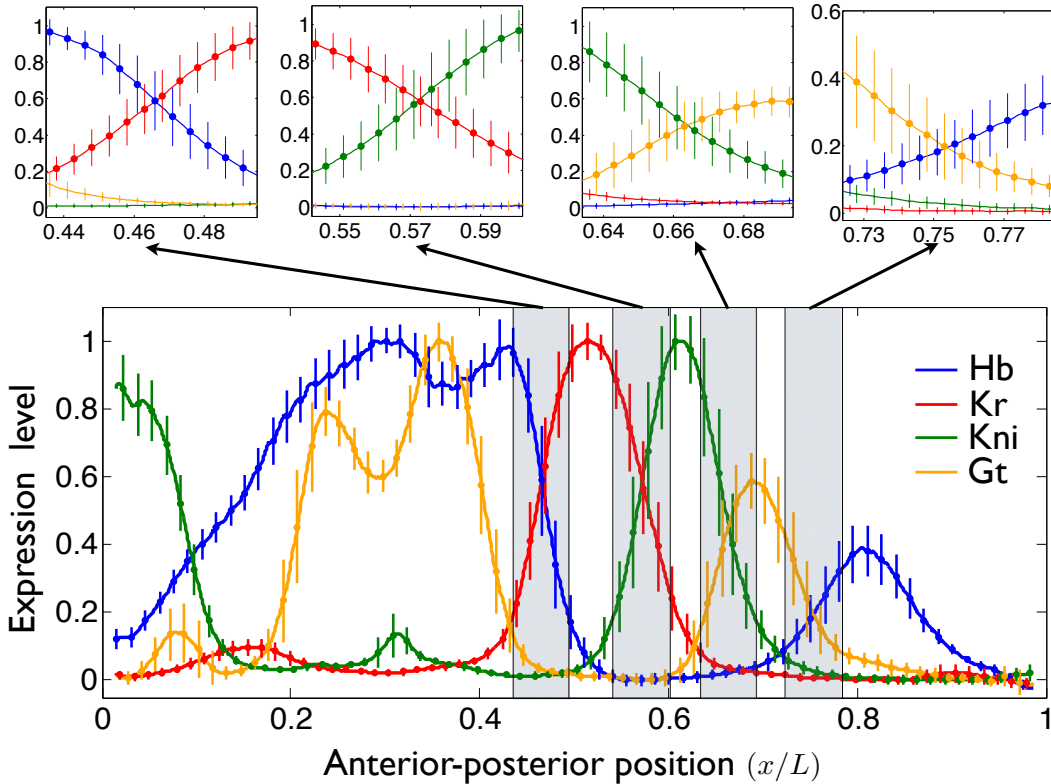


Figure 3.1: Normalized gap gene expression levels in the early *Drosophila* embryo, from Ref [11]. Measurements by simultaneous immunoflourescent staining of all four proteins, along the dorsal edge of the mid–saggital plane of the embryo, 38–49 min into nuclear cycle 14; error bars are standard deviations across $N = 24$ embryos. Upper left shows an expanded view of the shaded regions, near the crossings between Hb and Kr levels, where just these two genes have significant expression, and similarly for the Kr–Kni, Kni–Gt, and Gt–Hb crossings in upper panels from left to right.

We argue that criticality in a system of two mutually repressive genes generates several clear, experimentally observable signatures. First, there should be nearly perfect anti–correlations between the fluctuations in the two expression levels. As a

result, there are two linear combinations of the expression levels, or "modes," that have very different variances. Second, fluctuations in the large variance mode should have a significantly non–Gaussian distributions, while the small variance mode is nearly Gaussian. Third, there should be a dramatic slowing down of the dynamics along one direction in the space of possible expression levels. Finally, there should be correlations among fluctuations at distant points in the embryo. These signatures are related: the small variance mode will be the direction of fast dynamics, and under some conditions the large variance mode will be the direction of slow dynamics; the fast fluctuations should be nearly Gaussian, while the slow modes are non–Gaussian; and only the slow mode should exhibit long–ranged spatial correlations. We will see that all of these effects are found in the gap gene network. Importantly, these signatures do not depend on the molecular details.

## 3.2 Criticality in a network of two genes

To see that signatures of criticality are quite general, we consider a broad class of models for a genetic regulatory circuit. The rate at which gene products are synthesized depends on the concentration of all the relevant transcription factors, and we also expect that the gene products are degraded. To simplify, we ignore delays, so that the rate at which the protein encoded by a gene is synthesized depends instantaneously on the other protein (transcription factor) concentrations, and we assume that degradation obeys first order kinetics. We also focus on a single cell, leaving aside (for the moment) the role of diffusion. Then, by choosing our units correctly we can write the dynamics for the expression levels of two interacting genes as

$$\tau_1 \frac{dg_1}{dt} = f_1(c; g_1, g_2) - g_1 + \xi_1 \tag{3.1}$$

$$\tau_2 \frac{dg_2}{dt} = f_2(c; g_1, g_2) - g_2 + \xi_2, \tag{3.2}$$

where $g_1$ and $g_2$ are the normalized expression levels of the two genes, $\tau_1$ and $\tau_2$ are the lifetimes of the proteins, and $c$ represents the external (maternal) inputs. The functions $f_1$ and $f_2$ are the "regulation functions" that express how the transcriptional activity of each gene depends on the expression level of all the other genes; with our choice of units, the regulation function runs between zero (gene off) and one (full induction). All of the molecular details of transcriptional regulation are hidden in the precise form of these regulation functions [5], which we will not need to specify. Finally, the random functions $\xi_1$ and $\xi_2$ model the effects of noise in the system.

If the interactions are weak, then for any value of the external inputs $c$ there is a single steady state response, defined by expression levels $\bar{g}_1(c)$ and $\bar{g}_2(c)$. We can check whether this hypothesis is consistent by asking what happens to small changes in the expression levels around this steady state. We write $g_1 = \bar{g}_1 + \delta g_1$, and similarly for $g_1$, and then expand Eqs (3.1, 3.2) assuming that $\delta g_1$ and $\delta g_2$ are small. The result is

$$\frac{d}{dt} \begin{bmatrix} \delta g_1 \\ \delta g_2 \end{bmatrix} = \begin{bmatrix} -\Gamma_1 & \gamma_{12} \\ \gamma_{21} & -\Gamma_2 \end{bmatrix} \begin{bmatrix} \delta g_1 \\ \delta g_2 \end{bmatrix} + \begin{bmatrix} \eta_1 \\ \eta_2 \end{bmatrix} . \tag{3.3}$$

Here $\Gamma_1$ and $\Gamma_2$ are effective decay rates for the two proteins, which must be positive if the steady state we have identified is stable. The parameter $\gamma_{12}$ reflects the incremental effect of gene 2 on gene 1—$\gamma_{12} < 0$ means that the protein encoded by gene 2 is a repressor of gene 1—and similarly for $\gamma_{21}$. The noise terms $\eta_1$ and $\eta_2$ play the same role as $\xi_1$ and $\xi_2$, but have different normalization.

If the steady state that we have identified is stable, then the matrix

$$\hat{M} \equiv \begin{bmatrix} -\Gamma_1 & \gamma_{12} \\ \gamma_{21} & -\Gamma_2 \end{bmatrix} \tag{3.4}$$

must have two eigenvalues with negative real parts. This is guaranteed if the interactions are weak ($\gamma_{12}, \gamma_{21} \to 0$), but as the interactions become stronger it is possible for

35

one of the eigenvalues to vanish. This is the critical point. Notice that we can define the critical point without giving a microscopic description of all the interactions that determine the form of the regulation functions.

The linearized Eqs (3.3) predict that the relaxation of average expression levels to their steady states can be written as combinations of two exponential decays,

$$
\begin{bmatrix} \langle g_1(t) \rangle \\ \langle g_2(t) \rangle \end{bmatrix} = \begin{bmatrix} \bar{g}_1(c) \\ \bar{g}_2(c) \end{bmatrix} + \begin{bmatrix} A_{1s} & A_{1f} \\ A_{2s} & A_{2f} \end{bmatrix} \begin{bmatrix} e^{\Lambda_s t} \\ e^{\Lambda_f t} \end{bmatrix} \tag{3.5}
$$

where $\Lambda_s$ and $\Lambda_f$ are the "slow" and "fast" eigenvalues of $\hat{M}$. Thus, while we measure the two expression levels, there are linear combinations of these expression levels— different directions in the $(g_1, g_2)$ plane—that provide more natural coordinates for the dynamics, such that motion along each direction is a single exponential function of time. As we approach criticality, the dynamics along the slow direction becomes very slow, so that $\Lambda_s \to 0$.

The linearized Eqs (3.3) also predict the fluctuations around the steady state. As we approach criticality, things simplify, and we find the covariance matrix

$$
\begin{bmatrix} \langle (\delta g_1)^2 \rangle & \langle \delta g_1 \delta g_2 \rangle \\ \langle \delta g_1 \delta g_2 \rangle & \langle (\delta g_2)^2 \rangle \end{bmatrix} \to \sigma^2 \begin{bmatrix} 1 & \Gamma_1/\gamma_{12} \\ \Gamma_1/\gamma_{12} & (\Gamma_1/\gamma_{12})^2 \end{bmatrix}, \tag{3.6}
$$

where $\sigma^2$ is the variance in the expression level of the first gene. As with the dynamics, there are two "natural" directions in the $(g_1, g_2)$ plane corresponding to eigenvectors of this covariance matrix (principal components). In this linear approximation, the critical point is the point where we "lose" one of the dimensions, and the fluctuations in the two expression levels become perfectly correlated or anti–correlated. In addition, the direction with small fluctuations is the direction of fast relaxation.

## 3.3 Signatures of criticality in the data

Testing the predictions of criticality requires measuring the time dependence of gap gene expression levels, with an accuracy better than the intrinsic noise levels of the system. Absent live movies of the expression levels, the progress of cellularization provides a clock that can be used to mark the time during nuclear cycle fourteen at which an embryo was fixed [30], accurate to within one minute [11]. Fixed embryos, with immunofluorescent staining of the relevant proteins, thus provide a sequence of snapshots that can be placed accurately along the time axis of development. Immunofluorescent staining itself provides a measurement of relative protein concentrations that is accurate to within $\sim 3\%$ of the maximum expression levels in the embryo [11].

In Fig 3.2a we show the correlations between fluctuations in pairs of gap genes at each position. Gap gene expression levels plateau at $\sim 40\,\mathrm{min}$ into nuclear cycle fourteen [11], and the mean expression levels are shown as a function of anterior–posterior position in Fig 3.1. At each position we can look across the many embryos in our sample, and analyze the fluctuations around the mean, as in Ref [12]. We see that, precisely in the "crossing region" where Hb and Kr are the only genes with significant expression (marked A in Fig 3.2a), the correlation coefficient approaches $C = -1$, perfect (anti–)correlation, as expected at criticality. This pattern repeats at the crossing between Kr and Kni (B), at the crossing between Kni and Gt (C), and, perhaps less perfectly[1], at the crossing between Gt and Hb (D). These strong anti–correlations are shown explicitly in Fig 3.2b, where we plot the two relevant gene expression levels against one another at each crossing point. In all cases, the direction of small fluctuations is along the positive diagonal, while the large fluctuations are along the negative diagonal.

---

[1]Since we observe substantial anti–correlations both in the Gt–Hb pair and in the Hb–Kni pair, it is likely that the system is more nearly three dimensional in the neighborhood of this crossing, so that no single pair can achieve perfect correlation.
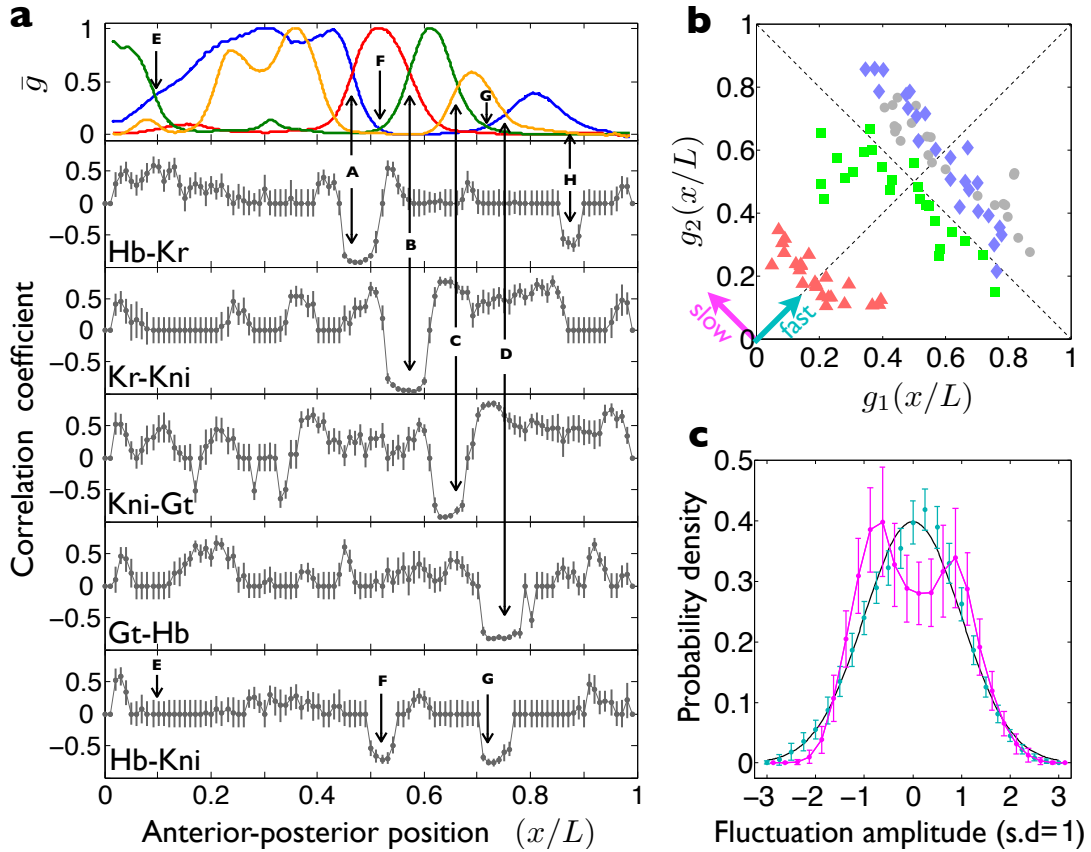
Figure 3.2: Fluctuations in gap gene expression levels. (a) Pairwise correlation coefficients between fluctuations in the different gap genes vs. anterior–posterior position, from the same data as in Fig 3.1. Mean expression levels at top to guide the eye, colors as in Fig 3.1; error bars are from bootstrap analysis. Correlations which are not significant at $p = 0.01$ are shown as zero. Major crossing points of the mean expression profiles are labelled A, B, C, and D; other points marked as described in the text. (b) Scatter plot of expression levels for pairs of genes in individual embryos: Kr vs Hb at point A (grey circles), Kni vs Kr at point B (blue diamonds), Gt vs Kni at point C (green squares), and Hb vs Gt at point D (red triangles). (c) Probability distribution of expression fluctuations. In each of the crossing regions from Fig 1, we form the combinations $\delta g_f$ (fast modes, cyan) and $\delta g_s$ (slow modes, magenta), and normalize the fluctuations across embryos to have unit variance at each position. Data from all four regions are pooled to estimate the distributions; error bars are from random divisions of the set of 24 embryos. Gaussian distribution (black) shown for comparison.

It is important that the strong anti–correlations tell us something about the underlying network, rather than being a necessary (perhaps even artifactual) corollary of the mean expression profiles. A notable feature of Fig 3.2a thus is what happens away from the major crossing points. There is a Hb–Kni crossing at $x/L = 0.1$ (E), but this does not have any signature in the correlations, perhaps because spatial variations in expression levels at this point are dominated by maternal inputs rather than being intrinsic to the gap gene network [43, 25]. This is evidence that we can have crossings without correlations, and we can also have correlations without crossings, as with Hb and Kr at point H; interestingly, H marks the point where an additional posterior Kr stripe appears during gastrulation [17, 14]. We also note that strong correlations can appear when expression levels are very small, as with Hb and Kni at points F and G; there also are extended regions of positive Kr–Kni and Kni–Gt correlations in parts of the embryo where the expression levels of Kr and Kni both are very low. Taken together, these data indicate that the pattern of correlations is not simply a reflection of the mean spatial profiles, but an independent measure of network behavior.

If we transfrom Eq (3.3) to a description in terms of the fast and slow modes $g_f$ and $g_s$, then precisely at criticality there is no "restoring force" for fluctuations in $g_s$ and formally the variance $\sigma^2$ in Eq (3.6) should diverge. This is cut off by higher order terms in the expansion of the regulation functions around the steady state, and this leads to a non–Gaussian distribution of fluctuations in $g_s$. Although the data are limited, we do find, as shown in Fig 3.2c, that fluctuations in the small variance (fast) direction are almost perfectly Gaussian, while the large variance (slow) direction show significant departures form Gaussianity, in the expected direction.

The time dependence of Hb and Kr expression levels during nuclear cycle fourteen is shown, at the crossing point $x/L = 0.47$, in Fig 3.3. Criticality predicts that if we take a linear combination of these expression levels corresponding to the direction
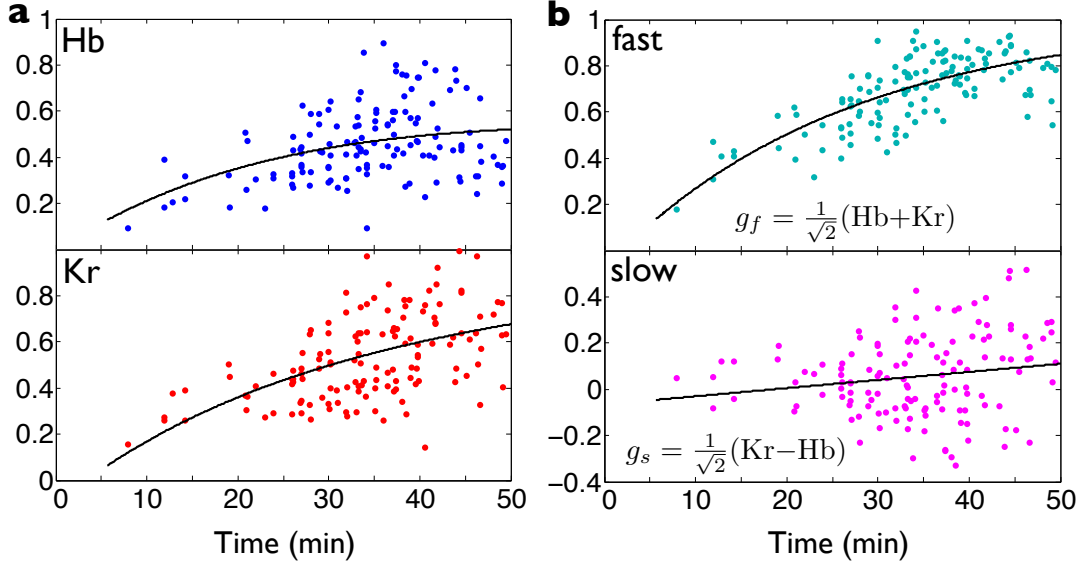
Figure 3.3: Dynamics at the Hb–Kr crossing point. (a) Normalized expression levels of the individual genes, plotted vs. time during nuclear cycle fourteen; data from Ref [11]. (b) Linear combinations of expression levels corresponding to the small variance (fast) and large variance (slow) directions in Fig 3.2b. Curves are best fit single exponentials for each mode and are also shown projected back into the individual expression levels in (a). Eigenvalues, as in Eq (3.5), are $\Lambda_f = -0.04 \pm 0.01 \, \text{min}^{-1}$ and $\Lambda_s = -0.002 \pm 0.007 \, \text{min}^{-1}$.

of small fluctuations in Fig 3.2b (cyan), then we will see relatively fast dynamics, and this is what we observe. In contrast, if we project onto the direction of large fluctuations (magenta), we see only very slow variations over nearly one hour. Indeed, the expression level along this slow direction seems almost to diffuse freely, with growing variance rather than systematic evolution. Thus, strong (anti–)correlations are accompanied by a dramatic slowing of the dynamics along one direction in the space of possible expression levels, and a similar pattern is found at each of the crossings, Kr–Kni, Kni–Gt, and Gt–Hb (data not shown). Again, this is consistent with what we expect for two–gene systems at criticality.

If we move along the anterior-posterior axis in the vicinity of the crossing point, the sum of expression levels of two genes, which is proportional to the fast mode, remains approximately constant, while the difference, which is proportional to the slow mode, changes. Therefore the dynamics of the slow mode, shown in Fig 3.3, will

generate motion of the pattern along the anterior–posterior axis. This slow shift is well known [11, 21].

The slow dynamics associated with criticality also implies that correlations should extend over long distance in space. As is clear from Fig 3.3, the eigenvalues $\Lambda_s$ and $\Lambda_f$ define time scales $\tau_s = -1/\Lambda_s$ and $\tau_f = -1/\Lambda_f$. If we add diffusion to the dynamics in Eqs (3.3), then these time scales define length scales, through the usual relation $\ell_{s,f} = \sqrt{D\tau_{s,f}}$; although there is some dependence on details of the underlying model, these lengths define the distances over which we expect fluctuations to be correlated. In particular, as we approach criticality, $\Lambda_s$ vanishes and the associated correlation length $\ell_s$ can become infinitely long, limited only by the size $L$ of the embryo itself. Searching for these long–ranged correlations is complicated by the fact that the system is inhomogeneous, but we have a built in control, since we should see the long ranged correlations only in the slow, large variance mode $\delta g_s$, and not in $\delta g_f$. This control also helps us discriminate against systematic errors that might have generated spurious correlations.

In Fig 3.4a we show the normalized correlation function

$$C_{ss}(x,y) = \frac{\langle \delta g_s(x)\delta g_s(y)\rangle}{(\langle[\delta g_s(x)]^2\rangle\langle[\delta g_s(y)]^2\rangle)^{1/2}}, \tag{3.7}$$

with $x$ held fixed at the Hb–Kr crossing and $y$ allowed to vary. We see that this correlation function is essentially constant throughout the crossing region. In contrast, the same correlation computed for the fast mode decays rapidly, with a length constant $\xi/L \sim 0.02$, just a few nuclear spacings along the anterior–posterior axis.

The dominant slow mode corresponds to different combinations of expression levels in different regions of the embryo. Generally, we can write the slow mode as a weighted
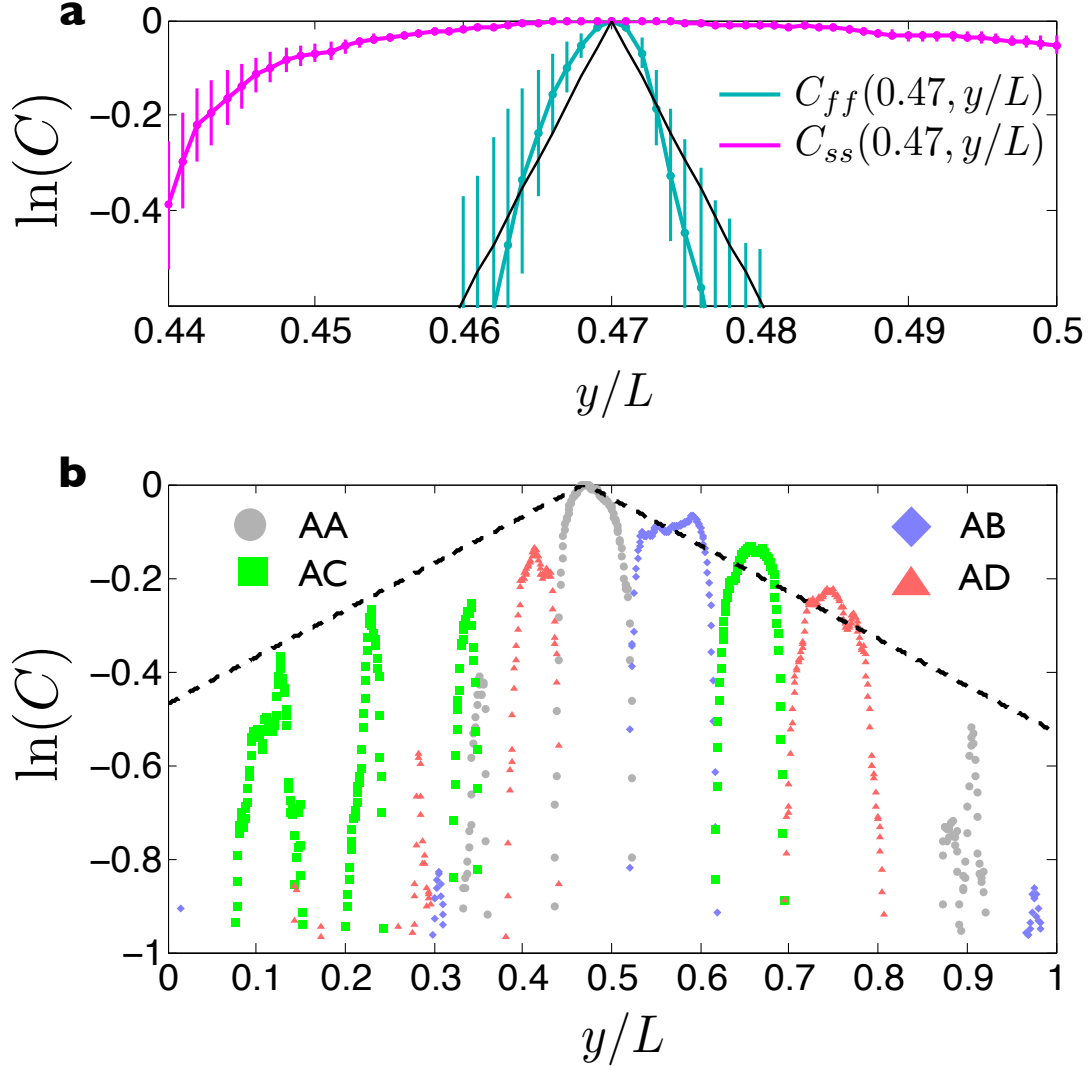
Figure 3.4: Spatial correlations of fluctuations in gene expression. (a) Auto–correlations of slow (magenta) and fast (cyan) modes near the Hb–Kr crossing, as defined in Eq (3.7). Line shows a fit, $C_{ff}(x,y) \propto e^{-|x-y|/\xi}$, with $\xi/L = 0.015 \pm 0.002$. (b) Correlations between the slow mode at the Hb–Kr crossing and slow modes at other crossings, as defined in Eq (3.10), indicated by the colors. All correlation functions are evaluated at $x/L = 0.47$ with $y$ varying as shown. Middle peak is the same (auto–)correlation function $C_{ss}$ as in (a). Dashed line is $e^{-|x-y|/\xi}$, with $\xi = L$.

sum of the different expression levels,

$$g_s(x) = \sum_{i=1}^{4} W_i(x) g_i(x), \tag{3.8}$$

where we label the gap genes i $=$ 1 for Hb, i $=$ 2 for Kr, i $=$ 3 for Kni, and i $=$ 4 for Gt. Near the Hb–Kr crossing, labelled A in Fig 3.2a, we have $W_i \approx W_i^A$, where $W_i^A$ are the weights that give us the anti–symmetric combination of Hb and Kr, as drawn in Fig 3.2b: $W_1^A = -1/\sqrt{2}$, $W_2^A = 1/\sqrt{2}$, and $W_3^A = W_4^A = 0$. Similarly, near the Kr–Kni crossing, labelled B in Fig 3.2a, we have $W_i \approx W_i^B$ with $W_2^B = -1/\sqrt{2}$, $W_3^B = 1/\sqrt{2}$, and $W_1^B = W_4^B = 0$, and this generalizes to crossing regions C and D. Using these weights, we obtain approximations to the slow mode,

$$\begin{bmatrix} g_s^A(y) \\ g_s^B(y) \\ g_s^C(y) \\ g_s^D(y) \end{bmatrix} = \sum_{i=1}^{4} \begin{bmatrix} W_i^A g_i(y) \\ W_i^B g_i(y) \\ W_i^C g_i(y) \\ W_i^D g_i(y) \end{bmatrix}, \tag{3.9}$$

and we expect that these approximations are accurate in their respective crossing regions. Now we can test for correlations over longer distances by computing, for example,

$$C_{ss}^{AB}(x,y) = \frac{\langle \delta g_s^A(x) \delta g_s^B(y) \rangle}{(\langle [\delta g_s^A(x)]^2 \rangle \langle [\delta g_s^B(y)]^2 \rangle)^{1/2}}, \tag{3.10}$$

holding $x/L = 0.47$ in the crossing region $A$ while letting $y$ vary through the crossing region $B$, and similarly for $C_{ss}^{AC}(x,y)$ and $C_{ss}^{AD}(x,y)$. The results of this analysis are shown in Fig 3.4b; note that $C_{ss}^{AA}(x,y)$ is the correlation we have plotted in Fig 3.4a.

Figure 3.4b shows that the slow mode is correlated over very long distances. We can see, for example, in $C_{ss}^{AC}$, correlations between fluctuations in expression level at the Hb–Kr crossing region and at the Kni–Gt crossing region, despite the fact that these regions are separated by $\sim 20\%$ of the length of the embryo and have no

significantly expressed genes in common. These peaks in the correlation functions appear also at points anterior to the crossing regions, presumably at places where our approximations in Eq (3.9) come close to some underlying slow mode in the network. The pattern of correlations has an envelope corresponding to an exponential decay with correlation length $\xi = L$ (dashed line in Fig 3.4b), and similar results are obtained for the correlation functions $C_{ss}^{BC}$, $C_{ss}^{BD}$, $C_{ss}^{CD}$, etc.. This means that fluctuations in expression level are correlated along essentially the entire length of the embryo, as expected at criticality.

## 3.4   Conclusions

To summarize, the patterns of gap gene expression in the early *Drosophila* embryo exhibit several signatures of criticality: near perfect anti–correlations of fluctuations in the expression levels of different genes at the same point, non–Gaussian distributions of the fluctuations in the large variance modes, slowing down of the dynamics of these modes, and spatial correlations of the slow modes that extend over a large fraction of the embryo. While each of these observations could have other explanations, the confluence of results strikes us as highly suggestive. Note that we have focused on aspects of the data that are connected to the hypothesis of criticality in a very general way, independent of other assumptions, rather than trying to build a model for the entire network.

The possibility that biological systems might be poised near critical points, often discussed in the past [2], has been re–invigorated by new data and analyses on systems ranging from ensembles of amino acid sequences to networks of neurons to flocks of birds [36]. In the specific context of transcriptional regulation, the approach to criticality serves to generate long time scales, which may serve to reduce noise and optimize information transmission [46]. For the embryo in particular, these long time

scales and the corresponding long length scales may give us a different view of the problem of scaling expression patterns to variations in the size of the egg [50, 3].

Even leaving aside the possibility of criticality, the aspects of the data that we have described here are not at all what we would see if the gap gene network is described by generic parameter values. There must be something about the system that is finely tuned in order to generate such large differences in the time scales for variation along different dimensions in the space of expression levels, or to insure that correlations are so nearly perfect and extend over such long distances.

# Chapter 4

# Effective theory for the zero mode

As is familiar from many examples in physics, for systems near the critical point, it might be useful to integrate out the heavy excitations from the microscopic equations of motion, and obtain an effective theory for the strongly fluctuating mode - the zero mode or order parameter. This effective equations are usually given by the Landau-Ginsburg theory. One important insight from the previous discussion is that criticality in the developing embryo does not exactly copy the standard examples from physics textbooks. As we explained in the previous chapter, the order parameter in the former case is a linear combination of physical degrees of freedom (the expression levels of the gap genes), but which genes enter this linear combination - depends on the position along the embryo. In other words the microscopic composition of the order parameter changes as we move along the anterior-posterior axis. Is it possible to write a general effective field theory for the zero mode in this situation? Can this theory teach us anything interesting about the development of fruit flies? These are the questions that we discuss in this chapter.

It turns out that for proper treatment of this problem we will have to introduce gauge fields into our equations. These gauge fields produce observable contributions to Green functions of the zero mode. The central result of this chapter is that the

normalized two point correlation function of the order parameter, for the network on $N$ genes, is given by the action of a relativistic particle moving on the product space of the $N-1$ dimensional sphere and the anterior-posterior axis of the fruit fly. We start with the theory, and compare it with experiments at the end of the chapter.

## 4.1  Theory

Let's again start with equations similar to (3.1,3.2), but now include diffusion. For the network of $N$ genes we have

$$\dot{g}_\alpha = F_\alpha\big(\{g_\beta\}; c\big) + \tilde{D}\ \partial_x^2\big(g_\alpha\big) \tag{4.1}$$

Here the functions $F_\alpha\big(\{g_\beta\}; c\big)$ are responsible for all the production and degradation processes of transcription factors, and we also assume that the proteins can diffuse with some diffusion coefficient $\tilde{D}$ that is assumed to be equal for all the transcription factors. In the steady state we have expression profiles $\bar{g}_\alpha(x)$ which satisfy

$$F_\alpha\big(\{\bar{g}_\beta\}; c\big) + \tilde{D}\ \partial_x^2\big(\bar{g}_\alpha\big) = 0 \tag{4.2}$$

and for the dynamics of the fluctuations, $g_\alpha(t, x) = \bar{g}_\alpha(x) + \delta g_\alpha(t, x)$, we obtain

$$\delta\dot{g}_\alpha = M_{\alpha\beta}\delta g_\beta + \tilde{D}\ \partial_x^2\big(\delta g_\alpha\big), \qquad M_{\alpha\beta}(x) = \frac{\partial F_\alpha}{\partial g_\beta}\bigg|_{\bar{g}(x), c(x)} \tag{4.3}$$

The dynamical matrix $M_{\alpha\beta}(x)$ depends on the position along the embryo. Let's consider first a toy model example of a symmetric matrix. Then we can decompose it as

$$M_{\alpha\beta}(x) = \sum_{i=1}^{N} \psi_\alpha^i(x)\lambda^i(x)\psi_\beta^i(x) \tag{4.4}$$

where $\lambda^i$ and $\psi^i_\alpha$ are eigenvalues and eigenvectors of $M_{\alpha\beta}$. Since $M_{\alpha\beta}$ is symmetric, we have

$$\psi^i_\alpha \psi^j_\alpha = \delta^{ij} \tag{4.5}$$

First of all we would like to project Eq (4.3) onto the eigenmodes of the matrix $M_{\alpha\beta}$. In order to do this we need to multiply Eq (4.3) by $\psi^k_\alpha$ and introduce a new set of variables - the eigenfluctuations

$$g^k = \psi^k_\alpha \delta g_\alpha \tag{4.6}$$

We obtain

$$\dot{g}^k = \lambda^k g^k + \tilde{D}\psi^k_\alpha \partial^2_x \big(\delta g_\alpha\big) \tag{4.7}$$

The problem with this equation is that the eigenvectors $\psi^i_\alpha(x)$ depend on the position, therefore we can not commute the $x$-derivative and $\psi^k_\alpha$ in the last term. Thus, in order to rewrite Eq (4.3) in the covariant form with respect to latin indices we have to introduce a gauge connection.

The set of eigenvectors $\psi^i_\alpha$ form a complete basis in the space of fluctuations. Therefore we can decompose the spatial derivative of an eigenvector in this basis

$$\partial_x \psi^k_\alpha = A^{ki} \psi^i_\alpha \tag{4.8}$$

for some coefficients $A^{ki}$. If we differentiate the orthogonality constraint (4.5) with respect to $x$, we can find that the matrices $A^{ij}(x)$ must be antisymmetric at every point in space

$$A^{ij} + A^{ji} = 0 \tag{4.9}$$

Now we can introduce the covariant derivative

$$\psi^k_\alpha \partial_x \big(\delta g_\alpha\big) = \partial_x g^k - A^{ki} g^i = \big(Dg\big)^k \tag{4.10}$$

Applying this trick twice we can rewrite Eq (4.7) in the fully covariant form

$$\dot{g}^k = \lambda^k g^k + \tilde{D}\left(D^2 g\right)^k \qquad (4.11)$$

or more explicitly

$$\dot{g}^k = \lambda^k g^k + \tilde{D}\left[\partial_x^2 g^k - A^{ki}\partial_x g^i - \partial_x(A^{ki}g^i) + A^{ki}A^{il}g^l\right] \qquad (4.12)$$

The coefficients $A^{ij}$ play the familiar role of a gauge field. In the case of the symmetric matrix $M_{\alpha\beta}$ the gauge group is $O(N)$ for the network of $N$ genes. The gauge field is an element of the adjoint representation, and therefore should be an antisymmetric matrix, as was shown above.

Thus far we haven't made any assumptions, all that we did is to transform Eq (4.3) from the basis of genes (greek indices) to the basis of collective modes (latin indices). But these two systems of equations are completely equivalent. Now we would like to make a reduction to the effective theory for the zero mode. In order to do this let's assume that all the eigenvalues $\lambda^i$ ($i = 2...N$) are negative and large, and the eigenvalue $\lambda^1(x) = -\varepsilon(x)$, where $\varepsilon(x)$ is a small position-dependent function. We do not assume any specific sign of $\varepsilon(x)$. In the critical regime $\varepsilon(x)$ approaches zero everywhere along the anterior-posterior axis. In this limit all the fluctuations $g^i$ ($i = 2...N$) become small and $g^1$ becomes large. In order to find the effective theory for the zero mode we simply need to drop all the modes $g^i$ ($i = 2...N$) whose fluctuations are small and retain only terms that couple to $g^1$ in Eq (4.12). The result is

$$\dot{g}^1 = -m^2(x)g^1 + \tilde{D}\partial_x^2 g^1 \qquad (4.13)$$

where

$$m^2(x) = \varepsilon(x) + \tilde{D}\sum_{i=2}^{N}\left(A^{1i}\right)^2 \qquad (4.14)$$

49

Thus the effective equation for the zero mode is very similar to the original equation (4.7) but with a renormalized mass of the zero mode. This renormalization is important. It tells us that the effective mass of the zero mode comes from two sources: the bare mass $\varepsilon(x)$ - the local (in space) property of the transcriptional network - and the gauge field $A(x)$, which is non-zero only if the operating point of the transcriptional network is changing as we move along the anterior-posterior axis. The biological origin of this second term can be traced to the presence of the maternal morphogens inside the cell that break translational symmetry and induce coordinate dependence of the dynamical matrix. Another important point is that this correction to the mass is always positive. This means that the non-local effects that we discuss here can only increase the effective mass. If the bare mass were already positive, this would push the system further away from criticality. If the bare mass were negative, this would stabilize the system and push it towards criticality.

Finally, we would like to emphasize the analogies and contrasts of this effect with the Higgs mechanism. In the latter case a scalar field receives a non-zero vacuum expectation value because of the external potential. This non-zero vacuum expectation value produces the mass for the gauge field. In our problem the situation is exactly the opposite. The maternal morphogens break translational symmetry inside the cell and this induces a non-zero value of the gauge field. This background gauge field produces the contribution to the mass of the scalar field - the zero mode.

To analyze these effects in a more quantitative way it is nice to go back to Eq (4.13) and introduce a dynamic noise that mimics the stochastic effects of transcriptional activity in various parts of the cell. We assume that the noise is white and translationally invariant for simplicity

$$\langle \xi_\alpha(x,t) \rangle = 0 \qquad \langle \xi_\alpha(x_1,t_1)\xi_\beta(x_2,t_2) \rangle = \mathcal{N}\delta(x_1 - x_2)\delta(t_1 - t_2)\delta_{\alpha\beta}$$

From now on we assume that $\tilde{D} = 1$, for convenience. We also use the following notations for the order parameter, the corresponding eigenvectors and the noise:

$$\psi_\alpha(x) = \psi_\alpha^1(x), \qquad g(x,t) = g^1(x,t) = \psi_\alpha(x)\delta g_\alpha(x,t), \qquad \xi(x,t) = \psi_\alpha(x)\xi_\alpha(x,t)$$

Our goal is to find the two-point function of the zero mode, which satisfies

$$\partial_t g = -m^2(x)g + \partial_x^2 g + \xi(x,t), \tag{4.15}$$

averaged over the noise. We introduce two Green functions: one for the time-dependent problem

$$\left[\partial_t - \partial_x^2 + m^2(x)\right]\Delta(x,t|y,\tilde{t}) = \delta(t-\tilde{t})\delta(x-y), \tag{4.16}$$

and one for the static problem

$$\left[-\partial_x^2 + m^2(x)\right]G(x,y) = \delta(x-y). \tag{4.17}$$

One can transform Eq (4.16) into Fourier space over time. The corresponding Green function is then given by

$$\Delta(x,y,\omega) = \sum_{n=0}^{\infty} \frac{\varphi_n(x)\varphi_n^*(y)}{-i\omega + \sigma_n}, \tag{4.18}$$

where $\varphi_n(x)$ and $\sigma_n$ are eigenfunctions and eigenvalues of the static differential operator

$$\left[-\partial_x^2 + m^2(x)\right]\varphi_n(x) = \sigma_n\varphi_n(x). \tag{4.19}$$

Using this representation we can calculate the two-point function of the zero mode

$$\langle g(x,t)g(y,t)\rangle = \mathcal{N} \int dz d\tilde{t} \, \Delta(x,t|z,\tilde{t})\Delta(y,t|z,\tilde{t}) = \mathcal{N} \int dz \, \frac{d\omega}{2\pi} \, \Delta(x,z,\omega)\Delta(y,z,-\omega) =$$

$$= \mathcal{N} \sum_{n=0}^{\infty} \int \frac{d\omega}{2\pi} \, \frac{\varphi_n(x)\varphi_n^*(y)}{\omega^2 + \sigma_n^2} = \frac{\mathcal{N}}{2} \sum_{n=0}^{\infty} \frac{\varphi_n(x)\varphi_n^*(y)}{\sigma_n} = \frac{\mathcal{N}}{2} G(x,y).$$

$$(4.20)$$

Thus, the two-point function in the theory with the dynamic noise is equal to the Green function of the static differential operator (4.17), multiplied by $\mathcal{N}/2$. The first three equalities in (4.20) can be also interpreted as consequence of the fluctuation-dissipation theorem.

In order to solve (4.17) we will assume that the embryo is large so that the correct Green function is selected by the condition that $G(x,y) \to 0$ as the distance between $x$ and $y$ becomes large. In other words we neglect by the possible influence of the boundary conditions at the ends of the embryo on the pattern of correlations that we are trying to find. Since we do not know the explicit dependence of the effective mass on the position, we can not solve (4.17) exactly. However it is instructive to use quasiclassical approximation to find the main features of the solution. Quasiclassics is valid in this problem as long as $m(x)$ is a sufficiently slow varying function of the position. In this limit we obtain

$$G(x_1, x_2) = \frac{1}{2\sqrt{m(x_1)m(x_2)}} e^{-\int_{x_<}^{x_>} m(z)dz} \tag{4.21}$$

Our ultimate goal is to find a quantity analogous to (3.7). Using (4.20) and (4.21) we obtain, assuming that $y > x$,

$$C(x,y) = \frac{\langle \, g(x,t) \, g(y,t) \, \rangle}{\sqrt{\langle g(x,t)^2 \rangle \, \langle g(y,t)^2 \rangle}} = e^{-S(x,y)} \tag{4.22}$$

where

$$S(x,y) = \int_x^y m(z)dz = \int_x^y dz \sqrt{\sum_{k=2}^N \left(A^{1k}(z)\right)^2 - \lambda(z)} \qquad (4.23)$$

From now on we will assume that the lightest eigenvalue $\lambda(z) = \lambda^1(z) = -\varepsilon(z)$ of the dynamical matrix $M_{\alpha\beta}$ is slightly positive or is equal to zero. Using definition (4.8) we can express the gauge field through the eigenvectors as

$$A^{1k} = \psi_\alpha^k \partial_x \psi_\alpha \qquad (4.24)$$

By exploiting the completeness property of the eigenvectors

$$\sum_{k=1}^N \psi_\alpha^k \psi_\beta^k = \delta_{\alpha\beta}$$

and using that $A^{11} = 0$, we can rewrite the action as (in the last formula we restored the diffusion coefficient that was assumed to be equal to one in the previous formulas)

$$S(x,y) = \int_x^y dz \sqrt{\sum_{k=1}^N \psi_\alpha^k \psi_\beta^k \, \partial_z \psi_\alpha \partial_z \psi_\beta - \lambda(z)} = \int_x^y dz \sqrt{\left(\partial_z \psi_\alpha\right)^2 - \frac{\lambda}{\tilde{D}}} \qquad (4.25)$$

This last form has a very transparent geometrical meaning - this is the action of a relativistic particle on the $(N-1)$-dimensional sphere with "time" representing the motion along the anterior-posterior axis of the fruit fly embryo.

In principle, this action should be calculated along the real trajectory on $S^{N-1} \times [0, L]$ (product of the unit sphere by the anterior-posterior axis) that is dictated by the non-linear equations (4.2). To get a lower bound on this action it is however possible to calculate it on the geodesic trajectory - the shortest path connecting the

initial and the final state. In order to do this we introduce the "effective time"

$$\Delta\chi = \int_x^y \sqrt{\frac{\lambda(z)}{\tilde{D}}} dz \qquad (4.26)$$

and the angle between the initial and the final position of the particle on the sphere

$$\psi_\alpha(x)\psi_\alpha(y) = \cos(\Delta\phi) \qquad (4.27)$$

The action calculated on the geodesic is then equal to

$$S^{geodesic} = \sqrt{\left(\Delta\phi\right)^2 - \left(\Delta\chi\right)^2} \qquad (4.28)$$

This quantity gives the lower bound on the value of the action evaluated on the realistic trajectory of the gap genes, given the dependence $\lambda(x)$ and the initial and final positions on the sphere.

$$S^{gap} > S^{geodesic} \qquad (4.29)$$

Thus $e^{-S^{geodesic}}$ provides the upper bound on the behavior of the correlation coefficient (4.22), given the anterior-posterior position dependence of the zero eigenvalue $\lambda(z)$.

The general case of an arbitrary (non-symmetric) matrix $M_{\alpha\beta}$ can be treated in a similar way. We notice that it can be decomposed as

$$M_{\alpha\beta}(x) = \sum_{i=1}^N \zeta_\alpha^i(x)\lambda^i(x)\psi_\beta^i(x) \qquad (4.30)$$

so that now we have left and right orthogonal matrices $\zeta_\alpha^i(x)$ and $\psi_\beta^i(x)$. Multiplying Eq (4.3) by $\psi_\alpha^k$ we obtain

$$\dot{g}^k = \Pi^{ki}g^i + \tilde{D}\left(D^2 g\right)^k \qquad (4.31)$$

where the matrix of eigenvalues is now weighted with the overlap of the left and the right eigenvectors

$$\Pi^{ki} = \psi_\alpha^k \zeta_\alpha^i \lambda^i \tag{4.32}$$

After the reduction to the effective theory for the zero mode, we obtain exactly the same equations (4.13,4.14) as in the symmetric case, with $\lambda^1$ replaced by $\lambda^1 \psi_\alpha^1 \zeta_\alpha^1$.

## 4.2   Comparison with experiments

In the previous section we derived the relationship between the correlation functions of the order parameter and the motion of the particle on the unit sphere of expression levels, Eq (4.22, 4.28). In this section we will argue that the qualitative features predicted by these equations can be seen in the real data. We can construct the full covariance matrix of the network of four gap genes at every position along the anterior-posterior axis

$$C_{\alpha\beta}(x) = \langle \delta g_\alpha(x) \delta g_\beta(x) \rangle \tag{4.33}$$

At every position we can identify the linear combination of the four gap genes that has the largest variance. We will define the order parameter, see Eq (4.6), as this linear combination. Thus

$$g(x) = \psi_\alpha(x) \delta g_\alpha(x) \tag{4.34}$$

where $\psi_\alpha(x)$ now is the eigenvector of the covariance matrix. Now we can calculate experimentally the correlation coefficient (4.22). The result is shown in the lower panel of Fig. 4.1. From the previous analysis and from the diagonalization of the covariance matrix we know the eigenvectors $\psi_\alpha$ at the four underlined intersection
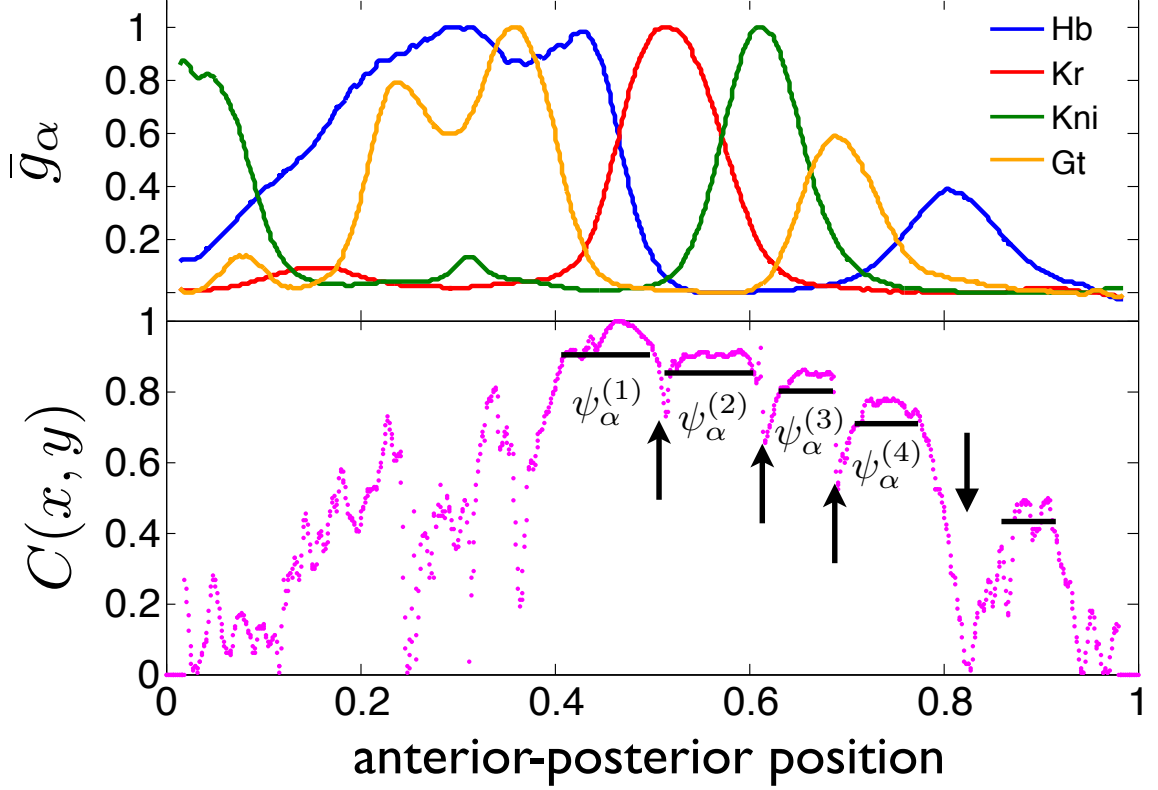
Figure 4.1: Top panel: mean expression profiles $\bar{g}_\alpha(x)$ of the four gap genes. Lower panel: auto-correlation coefficient $C(x, y)$ of the order parameter, defined as the mode with the largest variance. We keep $x = 0.47$ (the crossing point of Hb and Kr) and plot $C(x, y)$ as a function of $y$. This is a replotting of the spatial correlation graph from [27].

regions. They are approximately equal to

$$\psi_\alpha^{(1)} = \frac{1}{\sqrt{2}} \begin{pmatrix} -1 \\ 1 \\ 0 \\ 0 \end{pmatrix} \qquad \psi_\alpha^{(2)} = \frac{1}{\sqrt{2}} \begin{pmatrix} 0 \\ -1 \\ 1 \\ 0 \end{pmatrix} \qquad \psi_\alpha^{(3)} = \frac{1}{\sqrt{2}} \begin{pmatrix} 0 \\ 0 \\ -1 \\ 1 \end{pmatrix} \qquad \psi_\alpha^{(4)} = \frac{1}{\sqrt{2}} \begin{pmatrix} 1 \\ 0 \\ 0 \\ -1 \end{pmatrix}$$

$$(4.35)$$

throughout the underlined regions. In between, in the regions marked by the arrows, the eigenvectors presumably smoothly interpolate between the two values. These are the regions where we expect the gauge field to be non-zero. Within the underlined regions the gauge field is equal to zero.

56

Consider the following drastic approximation. Imagine that the lowest eigenvalue $\lambda(z)$ of the dynamical matrix is equal to zero everywhere along the anterior-posterior axis. As we will show in a moment this assumption is incorrect, but it is still useful to illustrate the logic. If that is true, the $\Delta\chi$ term in Eq (4.28) is equal to zero and the decay of the correlations is entirely determined by the variation of the eigenvector $\psi_\alpha$. Within the underlined regions in Fig. 4.1 this eigenvector does not change, therefore $S^{geodesic} = 0$ and the correlations should not decrease. In between the underlined regions, the eigenvector rotates, therefore the correlations should decrease. Qualitatively, this is precisely what the magenta curve in Fig. 4.1 looks like. It is relatively flat within the underlined regions, and there is a step-like decrease in the correlation once we transition from one plateau to the next. In principle, our approximation allows us to calculate the heights of the steps between the neighboring plateaus. The eigenvectors (4.35) are defined modulo reflections. We will assume that, as we move from the first plateau (corresponding to the eigenvector $\psi^{(1)}$) to the second plateau (corresponding to the eigenvector $\psi^{(2)}$), the eigenvector changes in such a way that the angle between the initial and the final states is minimal. In this specific example this means that if we start from $\psi^{(1)}$, the final eigenvector will be equal to $-\psi^{(2)}$ instead of $\psi^{(2)}$. The angle between the initial and the final vectors is then equal to

$$\Delta\phi = \frac{\pi}{3}$$

This means that the upper bound on the correlation coefficient within the region corresponding to the second plateau is equal to

$$C^{bound} = e^{-\pi/3} \approx 0.35$$

If our approximation were correct the real value of the correlation should be smaller than $C^{bound}$, because realistic trajectories do not have to coincide with geodesics.

Experimental value of the correlation in this region, however, is equal to $C \approx 0.9$, violating this bound.

Of course, the approximation that $\lambda(z) = 0$ is very naive and is motivated mostly by our inability to extract this quantity from the data. For the system to be critical what we really need is that the effective mass of the zero mode $m(z)$ is equal to zero, not that the "bare" mass $\lambda(z)$ equals zero. If our picture is correct, this observation suggests that in the absence of the non-local effects related to the rotation of the eigenvector $\psi_\alpha$ the transcriptional network is locally unstable. This corresponds to positive values of $\lambda(x)$ in the gaps between the neighboring plateaus. This positive contribution is compensated by the kinetic term for the vector $\psi$ in such a way that the total, effective, mass is close to zero. It would be interesting to see if future experiments can help to independently determine the dynamical matrix $M_{\alpha\beta}(x)$ and its lowest eigenvalue to test this prediction.

An alternative explanation for the violation of this bound is that the real network can be larger than the four genes that we discuss. If that is true, the angle between the initial and the final eigenvectors can be different from $\pi/3$. This can modify the heights of the steps. Again, it would be interesting to check experimentally if an additional gene, whose fluctuations are large and significantly contribute to the zero mode, exists and how it can modify the predictions of the theory regarding the correlations.

# Chapter 5

# Explicit examples of transcriptional networks

How difficult is it to tune a network to criticality? All the analyses that we discussed above do not rely on any specific model of transcriptional regulation. This is an advantage of this approach, since we don't know the microscopic details of what is happening at the promoters when multiple transcription factors bind to them. Having achieved this "model independent" understanding of the system, it is nice to go back and construct explicitly the regulatory networks within some broad class of models. A particularly attractive idea is to use the Monod-Wyman-Changeux (MWC) scheme [35], originally developed to describe the allosteric regulation of enzymes, to model the regulation machinery. Within this simple picture, we can calculate the regulation functions exactly and construct explicitly the phase diagram of all possible transcriptional networks that one can theoretically imagine. Can we now try to locate real embryos on this phase diagram? From the previous arguments we know that they must be located in the vicinity of the critical surfaces. But how densely is this region covered with hypothetical (theoretically designed) networks? Such a "model dependent" approach can help us to explore the space of all possible models and to

answer the question of how difficult it is to tune a network to criticality. In addition, such explicit models can be tested by comparing their predictions for the architecture of enhancers (number of binding sites) with ChIP/chip and other experimental data.

The text of this chapter was written jointly by D.Krotov and W.Bialek as part of an unpublished draft [26].

## 5.1   Taking a simple model seriously

In the previous chapters we worked with arbitrary activations functions $f_\alpha(c; \{g_\beta\})$ that enter equations (3.1,3.2). Now we need to specify the form of these functions. The Monod–Wyman–Changeux (MWC) model [35, 3], originally developed to describe allosteric regulation of enzymes, provides a simple physical picture within which we can calculate the regulation functions exactly (Fig 5.1). We imagine that the transcriptional apparatus for each gene has two states, active and inactive, and that switching between these states is fast enough that the effective rate of transcription is proportional to the probability of being in the active state. Each transcription factor that binds shifts the equilibrium between active and inactive states: activators lower the free energy of the active state relative to the inactive state, while repressors do the opposite. The key simplification of the MWC model is to assume that all the binding events are intrinsically independent; they interact, and binding becomes cooperative, only through the shifting equilibrium between the active and inactive states.

Imagine that in the enhancer region of gene $\alpha$ there are $\hat{N}_{\alpha\beta}$ binding sites for the transcription factor encoded by gene $\beta$, and these binding sites are described by dissociation constants $Q_{\alpha\beta}^{\text{on}}$ when the system is in the active state, and $Q_{\alpha\beta}^{\text{off}}$ when the system is in the inactive state; we could imagine a more complex model in which each of the binding sites had a different affinity, but we'll see that this isn't essential to the discussion. In a similar way, we imagine that the enhancer for gene $\alpha$ has $\hat{n}_\alpha$ binding
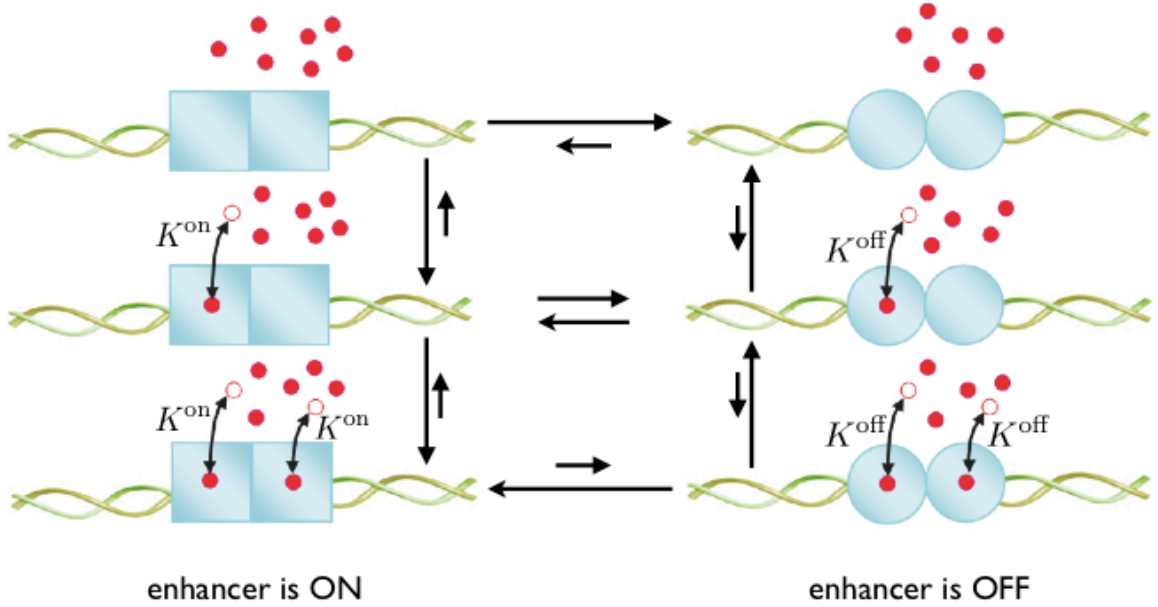
Figure 5.1: A schematic of an enhancer with two binding sites. The enhancer can exist in two states: ON or OFF . Transcription factors can bind to the two binding sites independently with dissociation constants $K^{\text{on}}$ and $K^{\text{off}}$. Assuming that the transcription factor (at external concentration $c$) is an activator, the equilibrium favors the OFF state when the binding sites are empty. However, binding is stronger to the ON state, $K^{\text{on}} \ll c \ll K^{\text{off}}$. Therefore, as more sites are occupied, the equlibrium shifts toward the ON state. The length of the arrows is proportional to the probability of transition between the states.

sites for the primary input morphogen, and these binding sites have dissociation constants $K_\alpha^{\text{on}}$ and $K_\alpha^{\text{off}}$ depending on whether the system is in the active or inactive state. If a transcription factor binds to the active and inactive states with different binding constants, then the binding event will shift the equilibrium between the two states.

Once we know the dissociation constant for each binding event, we can enumerate all the possible states of the system (occupied/unoccupied binding sites, active/inactive transcription) and give each state its appropriate Boltzmann weight on the assumption that binding reactions come to equilibrium. Finally, we can sum over all the different combinations of bound and unbound sites to obtain the effective free energy difference between active and inactive states, which determines the probability

$f_\alpha$ that the system is in the active state. The result is:

$$f_\alpha(\{g_\beta\}; c) = \frac{1}{1 + \exp\left[\theta'_\alpha - F_\alpha(\{g_\beta\}; c)\right]} \tag{5.1}$$

$$F_\alpha = \hat{n}_\alpha \ln\left(\frac{1 + c/K^{\text{on}}_\alpha}{1 + c/K^{\text{off}}_\alpha}\right) + \sum_\beta \hat{N}_{\alpha\beta} \ln\left(\frac{1 + g_\beta/Q^{\text{on}}_{\alpha\beta}}{1 + g_\beta/Q^{\text{off}}_{\alpha\beta}}\right) \tag{5.2}$$

where $F_\alpha$ is the part of the free energy (normalized by $k_B T$) that depends on the concentrations of the various regulators, and $\theta'_\alpha$ reflects the intrinsic free energy difference between active and inactive states.

If the transcription factor encoded by gene $\beta$ activates the expression of gene $\alpha$, then we must have $Q^{\text{on}}_{\alpha\beta} < Q^{\text{off}}_{\alpha\beta}$, which means that the transcription factor binds more strongly (with smaller dissociation constant) to the active state. If this difference in binding strengths is very large, then it is plausible that over some range of expression levels for the transcription factor we will have $Q^{\text{on}}_{\alpha\beta} \ll g_\beta \ll Q^{\text{off}}_{\alpha\beta}$. In this limit, we can approximate

$$\hat{N}_{\alpha\beta} \ln\left(\frac{1 + g_\beta/Q^{\text{on}}_{\alpha\beta}}{1 + g_\beta/Q^{\text{off}}_{\alpha\beta}}\right) \approx \hat{N}_{\alpha\beta} \ln g_\beta - \hat{N}_{\alpha\beta} \ln Q^{\text{on}}_{\alpha\beta} \tag{5.3}$$

In contrast, if the transcription factor encoded by gene $\beta$ is a repressor, we have $Q^{\text{on}}_{\alpha\beta} > Q^{\text{off}}_{\alpha\beta}$, and the limit analogous to Eq (5.3) becomes

$$\hat{N}_{\alpha\beta} \ln\left(\frac{1 + g_\beta/Q^{\text{on}}_{\alpha\beta}}{1 + g_\beta/Q^{\text{off}}_{\alpha\beta}}\right) \approx -\hat{N}_{\alpha\beta} \ln g_\beta + \hat{N}_{\alpha\beta} \ln Q^{\text{off}}_{\alpha\beta} \tag{5.4}$$

One can make a similar argument about the input morphogen, which we assume is an activator, so that

$$\hat{n}_\alpha \ln\left(\frac{1 + c/K^{\text{on}}_\alpha}{1 + c/K^{\text{off}}_\alpha}\right) \approx \hat{n}_\alpha \ln c - \hat{n}_\alpha \ln K^{\text{on}} \tag{5.5}$$

Putting all of these terms together, we have

$$F_\alpha \approx \text{constant} + n_\alpha \ln c + \sum_\beta N_{\alpha\beta} \ln g_\beta \tag{5.6}$$

where $N_{\alpha\beta} = \hat{N}_{\alpha\beta}$ if $\beta$ is an activator, and $N_{\alpha\beta} = -\hat{N}_{\alpha\beta}$ if $\beta$ is a repressor. Thus for the network of $M$ genes we have:

$$f_\alpha(\{g_\beta\}; c) = \frac{1}{1 + A_\alpha c^{-n_\alpha} g_1^{-N_{\alpha 1}} g_2^{-N_{\alpha 2}} \dots g_M^{-N_{\alpha M}}} \tag{5.7}$$

where the constants $A_\alpha$ are determined by the intrinsic free energy difference between the active and inactive states and the dissociation constants of all the transcription factors affecting gene $\alpha$. The absolute value of integers $|N_{\alpha\beta}|$ counts the number of binding sites, and the sign of $N_{\alpha\beta}$ distinguishes activators ($N_{\alpha\beta} > 0$) from repressors ($N_{\alpha\beta} < 0$).

The main focus of this chapter is the study of the mean expression profiles within the crossing regions of the neighboring gap genes. As we will see in a moment, the spatial profiles in these regions are well approximated by linear functions. Since the Laplacian operator gives zero when it acts on a linear function, we will ignore the effects of diffusion throughout this section. Therefore we discuss the following equations

$$\tau_\alpha \frac{dg_\alpha}{dt} = f_\alpha(\{g_\beta\}; c) - g_\alpha \tag{5.8}$$

Using the explicit expressions for the activation functions (5.7) we can calculate the dynamical matrix

$$M_{\alpha\beta}(x) = \left. \frac{\partial f_\alpha}{\partial g_\beta} \right|_{\bar{g}(x), c(x)} - \delta_{\alpha\beta} \tag{5.9}$$

Using that in the steady state the expression profiles satisfy $f_\alpha(\{\bar{g}_\beta\}; c) = \bar{g}_\alpha$, we obtain

$$M_{\alpha\beta} = N_{\alpha\beta}\frac{\bar{g}_\alpha}{\bar{g}_\beta}(1 - \bar{g}_\alpha) - \delta_{\alpha\beta} \tag{5.10}$$

What is important about Eq (5.10) is that, in the limits we are considering, the dynamical matrix depends only on the expression levels themselves and on the numbers of binding sites for the transcriptions factors. The numbers of binding sites $N_{\alpha\beta}$ provide a measure for the strength of the interactions, and when these interactions are weak ($N_{\alpha\beta} \to 0$) any steady state is stable. Importantly, the condition for criticality—the point where one of the eigenvalues of $M_{\alpha\beta}$ vanishes—then defines a relationship among the expression levels of the different genes: given the parameters $N_{\alpha\beta}$, the critical surface becomes a surface in the space of expression levels.

## 5.2 Zooming in on the Hb-Kr crossing

As we move from the anterior to the posterior of the *Drosophila* embryo, there is a region near the point where the mean expression levels of Hb and Kr cross, where just these two genes have significant expression levels (see 3.1). In this region, it makes sense to consider a model of just two interacting genes, driven by maternal input from Bicoid. In this case Eq (5.8) become more explicitly,

$$\tau_1 \frac{dg_1}{dt} = f_1(g_1, g_2, c) - g_1 \tag{5.11}$$

$$\tau_2 \frac{dg_2}{dt} = f_2(g_1, g_2, c) - g_2 \tag{5.12}$$

where $g_1$ refers to the expression level of Hb and $g_2$ refers to the expression level of Kr; the external input is provided by Bcd, which is at concentration $c$. These equations describe the dynamics of expression in one nucleus, and each nucleus along the length of the embryo has a different value of $c$, following the Bcd gradient.
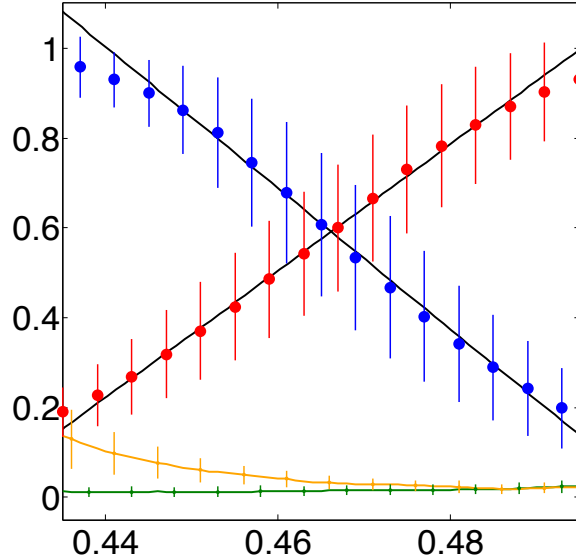
Figure 5.2: Zoomed in expression levels of Hb (blue) and Kr (red) with Kni (green) and Gt (yellow) as a function of the anterior–posterior axis of the embryo. Black lines - linear fits to the data - are good descriptions of the profiles over roughly $10 - 90\%$ of the full dynamic range

If the spatial profiles of gap gene expression reach a steady state, then Eqs (5.11, 5.12) predict that

$$\bar{g}_1(x) \quad = \quad f_1(\bar{g}_1(x), \bar{g}_2(x), c(x)) \tag{5.13}$$

$$\bar{g}_2(x) \quad = \quad f_2(\bar{g}_1(x), \bar{g}_2(x), c(x)) \tag{5.14}$$

where now we make the spatial dependence of all expression levels explicit, along with that of the input morphogen, Bicoid. It is striking that, near the Hb–Kr crossing point, the spatial profiles of gene expression are very well approximated as linear; straight lines are good descriptions of the profiles over roughly $10 - 90\%$ of the full dynamic range (Fig 5.2). Thus it is interesting to ask what our model predicts about the slopes of the expression levels near the crossing. Since Eq (5.13,5.14) should be satisfied for every $x$ along the anterior–posterior axis, we can differentiate them, remembering that all the expression levels $\{g_\alpha\}$ and the concentration $c$ of the primary

morphogen depend on $x$. Thus, we obtain

$$
\begin{bmatrix} M_{11} & M_{12} \\ M_{21} & M_{22} \end{bmatrix} \begin{bmatrix} s_1 \\ s_2 \end{bmatrix} = \begin{bmatrix} \frac{\partial f_1}{\partial c} \\ \frac{\partial f_2}{\partial c} \end{bmatrix} \begin{bmatrix} -\frac{dc(x)}{dx} \end{bmatrix} \tag{5.15}
$$

where $s_1 = dg_1/dx$ is the spatial slope of Hb expression, and similarly $s_2 = dg_2/dx$ is the spatial slope of Kr expression. Importantly, the matrix $M_{\alpha\beta}$ that appears here is the same dynamical matrix that appeared above.

The MWC model also gives us an explicit expression for the terms $\partial f_\alpha/\partial c$, in the same limits as above,

$$
\frac{\partial f_\alpha}{\partial c} = \frac{n_\alpha}{c} \bar{g}_\alpha (1 - \bar{g}_\alpha) \tag{5.16}
$$

where there are $n_\alpha$ binding sites for the input morphogen on the enhancer for gene $\alpha$. Experimentally, the spatial profile of Bicoid concentration is approximately exponential, $c(x) = c_0 e^{-x/\ell}$, so that $dc(x)/dx = -c(x)/\ell$. Finally, since we are expanding around the crossing point, we have $\bar{g}_1 = \bar{g}_2 = g_0$. Putting all of these pieces together, we have

$$
\begin{bmatrix} -1 + N_{11}(1 - g_0) & N_{12}(1 - g_0) \\ N_{21}(1 - g_0) & -1 + N_{22}(1 - g_0) \end{bmatrix} \begin{bmatrix} s_1 \\ s_2 \end{bmatrix} = A \begin{bmatrix} n_1 \\ n_2 \end{bmatrix} \tag{5.17}
$$

where $A = -g_0(1 - g_0)/\ell$.

Equation (5.17) predicts relationships among four measurable quantities: the expression level ($g_0$) and two slopes ($s_1, s_2$) at the Hb–Kr crossing, and the length constant ($\ell$) of the Bicoid profile. If, for example, we take the slopes as given, then every choice of the integers $N_{\alpha\beta}$ and $n_\alpha$ that defines the numbers of binding sites generates a prediction of the expression level and length constant, which we can plot as a point in the $(g_0, \ell)$ plane. But not all of the models are allowed, and hence not all points in the $(g_0, \ell)$ plane are consistent with the observed slopes. It is implausible that there are too many binding sites for one transcription factor on a single enhancer,
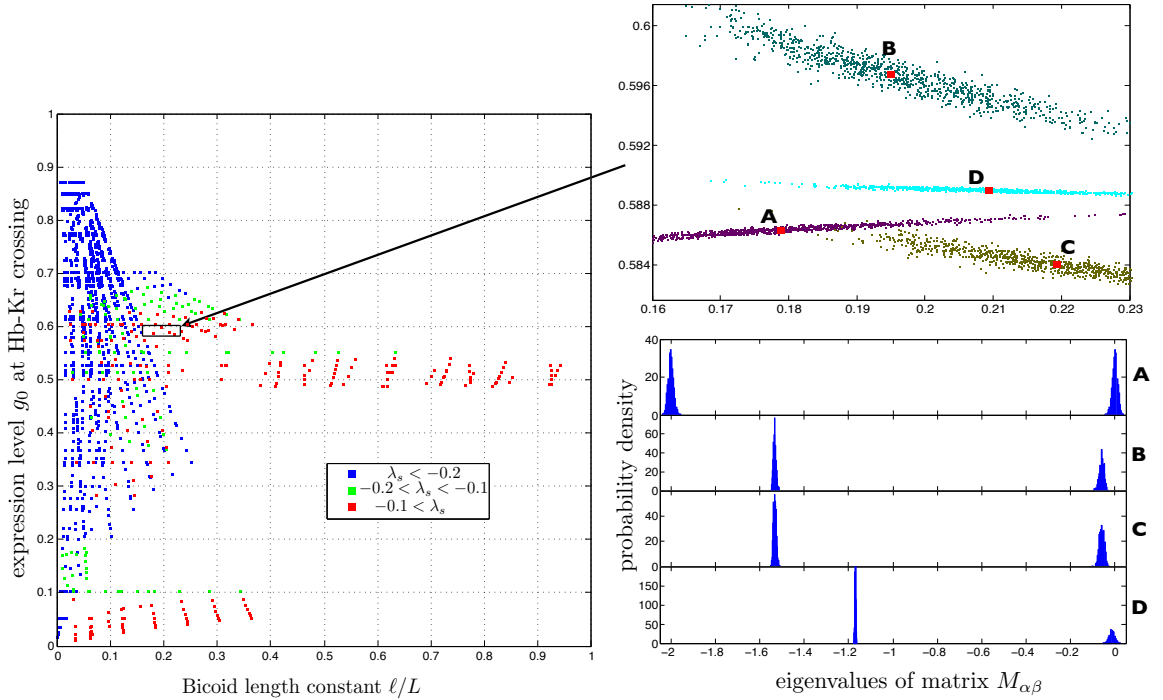
Figure 5.3: Exploring all possible MWC models for the HB–Kr crossing point. We work in the strong binding limit, and vary the numbers of binding sites $N_{\alpha\beta}$ and $n_\alpha$ from 0 to 6 (117649 models in total). Given the slopes of the expression levels in the neighborhood of the Hb–Kr crossing Eqs (5.18, 5.19), each model predicts the expression level $g_0$ at the crossing and the length constant, $\ell$ of the Bicoid gradient, from Eq (5.17). Each point on the left plot corresponds to a stable (in the region $0.45 < x/L < 0.48$) model (total 3014 models). The model is considered stable if the real parts of both eigenvalues of matrix $M_{\alpha\beta}$ are negative; in practice we retained the models with the smallest (in absolute value) eigenvalue $\lambda_s < +0.03$ to keep track of those models that are critical within the error bars. Each point is color coded according to the value of the smallest eigenvalue. The region of relevance to experiment ($0.16 < \ell/L < 0.23$ [32] and $0.582 < g_0 < 0.602$ from Fig 3.1) is shown by the black rectangle. There are 4 models that fall into it, which are shown in Table 5.1. We expand the region of relevance to experiment on the right panel, showing the 4 models that fit the data. Each model is now represented by a cloud of points, generated by drawing values of slopes $s_{1,2}$ from a random subset of embryos from the data set. Lower right panel shows the eigenvalues of the matrix $M_{\alpha\beta}$ for each of these models; the errors in our measurement of $g_0$ generate a distribution of results. Note that in each case the distribution of the smallest eigenvalue is concentrated very close to zero.

and we must also insist that the steady state predicted by the model is stable at the point where both expression levels are equal to the predicted $g_0$.

Because the spatial profiles of Hb and Kr are so nearly linear near their crossing point (see Fig. 5.2), the expression level at the crossing point ($g_0 = 0.59 \pm 0.005$ mean $\pm$ standard error of the mean) and the slopes

$$s_1 \equiv \frac{dg_{\text{Hb}}}{dx} = -\left(\frac{1}{L}\right)(15.75 \pm 0.45) \tag{5.18}$$

$$s_2 \equiv \frac{dg_{\text{Kr}}}{dx} = +\left(\frac{1}{L}\right)(14.11 \pm 0.36) \tag{5.19}$$

are really all we can extract from the profiles in this region. We note that all these quantities are determined with an accuracy of better than 3% if we focus on a single time point during development (here, $t = 42.7 \pm 3.1\,\text{min}$ from the start of nuclear cycle 14). For a more detailed discussion of accuracy in these measurements see Ref [11].

Taking the slopes of the profiles as given by Eqs (5.18) and (5.19), we can walk through all possible choices of the numbers $\{N_{\alpha\beta}, n_\alpha\}$, checking for stability in the region $0.45 < x/L < 0.48$, and then plot in the $(g_0, \ell)$ plane all the points that correspond to stable models; we restrict the number of binding sites to be less than six though precise limit for most of them is not important (see discussion below). We also restrict the mutual regulation to being repressive [19, 47, 18] or neutral ($N_{12} \leq 0$, $N_{21} \leq 0$), autoregulation to being positive [49, 47] or absent ($N_{11} \geq 0$, $N_{22} \geq 0$) and Bcd to being an activator [9, 10, 18] ($n_\alpha \geq 0$). The results of this calculation are shown in Fig 5.3. We see that in some regions of the $(g_0, \ell)$ plane, the points corresponding to stable models are very dense. In contrast, in the region of the plane that corresponds to what we actually find in the *Drosophila* embryo, stable models are quite sparse. Indeed, expanding the relevant region, we see that there are just a handful of possible models.

| model | $N_{11}$ | $N_{12}$ | $N_{21}$ | $N_{22}$ | $n_1$ | $n_2$ |
|-------|----------|----------|----------|----------|-------|-------|
| **A** | 0 | -2 | -3 | 0 | 3 | 4 |
| **B** | 1 | -1 | -3 | 0 | 3 | 4 |
| **C** | 1 | -1 | -3 | 0 | 3 | 5 |
| **D** | 1 | -1 | -2 | 1 | 3 | 4 |

Table 5.1: Models for the Hb–Kr crossing point, from Fig 5.3. Parameters are as described in the text: $N_{\alpha\beta}$ counts the number of binding sites on the enhancer of gene $\alpha$ for the transcription factor encoded by gene $\beta$, with the positive sign for activators and negative sign for repressors, and $n_\alpha$ counts the number of binding sites for Bicoid on the enhancer for gene $\alpha$. Gene 1 is *hunchback* and gene 2 is *krüppel*.

The conclusion from Fig 5.3 is that there are just a few models that are consistent with the observed combination of expression level, slopes, and input gradient that is observed near the Hb–Kr crossing point. These models are listed in Table 5.1. They are very special, since in each case if we look at the matrix $M_{\alpha\beta}$ we find that it has very nearly zero determinant, so that we are close to the critical surface. Note that in the absence of network interactions (all $N_{\alpha\beta} = 0$), both eigenvalues of $M_{\alpha\beta}$ are equal to $-1$, while criticality is the point where one of these eigenvalues crosses zero. Thus we can measure the approach to criticality by the size of the eigenvalue that is nearest to zero. Since the matrix $M_{\alpha\beta}$ depends on the expression level $g_0$ at the crossing point, the small errors in our measurement of this quantity propagate to give a distribution of eigenvalues in each model, and this is shown in Fig 5.3. We see that each of the models that are consistent with the data have eigenvalues that are within a few percent of zero, and thus are nearly critical.

## 5.3 Comparing the architecture of enhancers with experiments

The architecture of the gap gene enhancers has been extensivly studied in prior publications, which allows us to compare the models selected in our procedure with the

results of previous experiments. The Hb enhancer responsible for the patterning of the anterior part of the embryo is believed to have 3 strong binding sites of Bcd [9, 10]; the binding sites of Kr and Hb has been also reported [47]. The central domain enhancer of Kr is believed to have 5 Bcd binding sites and 1-6 Hb binding sites [18]. These numbers should be considered as upper limits, since some of the binding sites might be used for patterning of regions away from the crossing point. All these results are consistent with Table 5.1 which contains the numbers of binding sites in the strong binding approximation. Existence of clusters of binding sites have also been reported by high-throughput experiments [31]. The results are summarized in Fig. 5.4. The general conclusion is that the known enhancers of the gap genes have clusters of binding sites for all the four gap gene transcription factors as well as Bicoid. This results do not allow us to determine the number of binding sites within the clusters or the number of "functional" binding sites that are actually required for generation of the pattern.

Finally, in our selection procedure we restricted the number of binding sites to be fewer than 6 to make the computation feasible. It turns out that this upper limit can be relaxed for all the integers except $n_1$ without generation of additional models in the experimentally relevant window. Allowing more than 6 Bcd binding sites on the Hb promoter we can find other models, some of which are non-critical, in the experimentally relevant range of parameters.

## 5.4 Phase diagram in the space of expression levels

We can think of moving along the anterior–posterior axis of the embryo as tracing a trajectory through the space of expression levels. Focusing on Hb and Kr, the relevant space is a plane, and the trajectory is (roughly) a counterclockwise orbit (Fig 5.5): we start at the anterior end of the embryo where both expression levels are near zero,
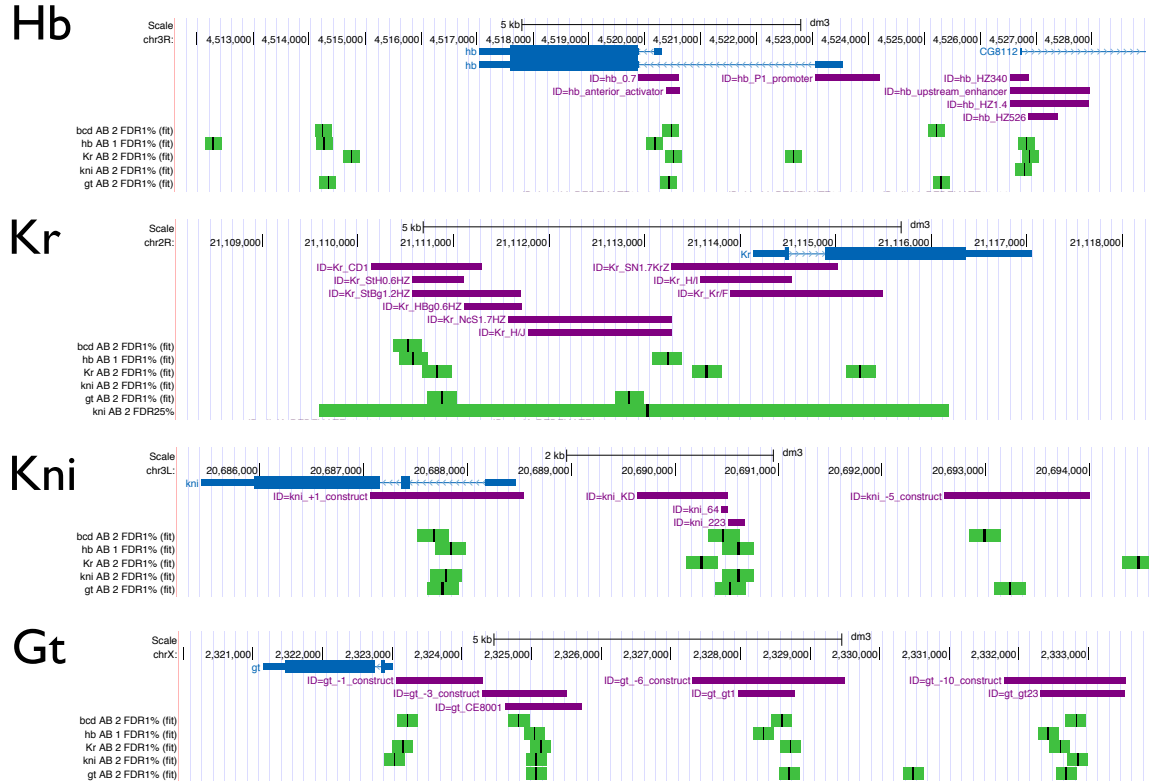
Figure 5.4: Clusters of binding sites from the ChIP/chip study [31]. Blue color represents the gene of interest, magenta denotes known CRMs associated with the gene, green represents the clusters of transcription factor binding sites.

then Hb rises to near its maximal value with Kr remaining near zero, then Kr rises as Hb falls, leading into the other corner of the plane, and Kr falls while Hb is near zero; after this loop, there is a second excursion to intermediate Hb levels as Kr remains near zero. But the condition for criticality—vanishing of one of the eigenvalues of the matrix $M_{\alpha\beta}$—also defines a trajectory through the space of expression levels, the "critical surface," and we can compute this surface for each of the models in Table 5.1; the results are shown in Fig 5.5, overlaid on the data. What we see is that the trajectory of expression levels in the embryo stays very close to the critical surface throughout the region where our two dimensional description makes sense.

It is worth emphasizing that the data follows the shape of the critical surface quite well and that our theoretical model does not have any continuous fitting parameters (it is parametrized by the set of integers $N_{\alpha\beta}$ only). If we now relax the assumption
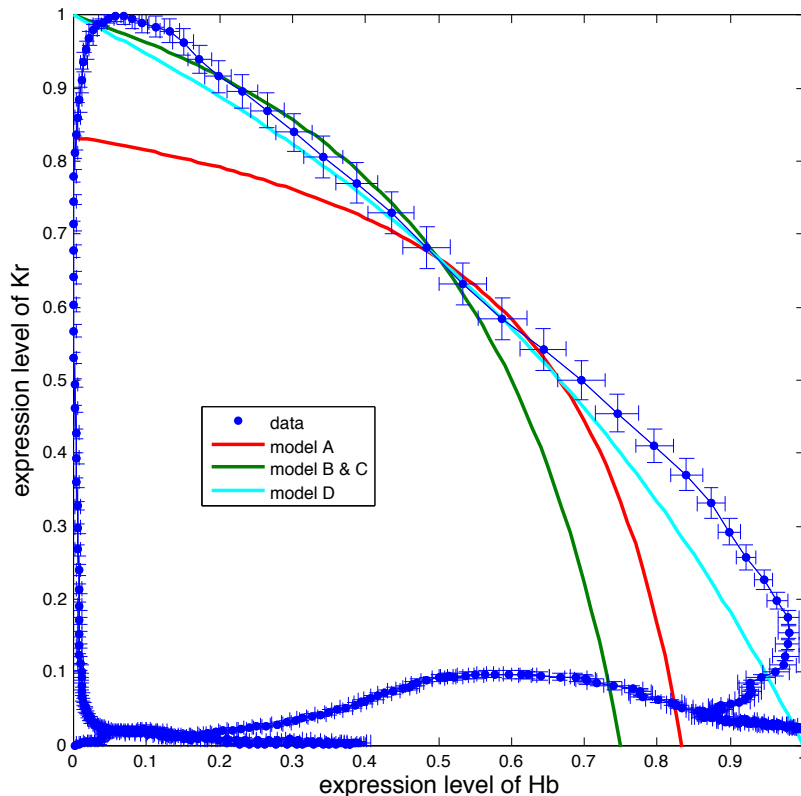
Figure 5.5: The trajectory of Krüppel vs Hunchback expression levels along the anterior–posterior axis of the embryo. This is a replotting of the data in Fig 3.1, emphasizing the "orbit" in expression space. For comparison we plot the critical surfaces $det(M) = 0$ for the four models in Table 5.1. We see that the real expression levels trace along the critical surface throughout much of the "crossing region" where just these two genes are expressed. Error bars are standard error of the mean.

of strong binding in our model, the dynamical matrix $M_{\alpha\beta}$ becomes

$$M_{\alpha\beta} = \frac{N_{\alpha\beta}\bar{g}_\alpha(1 - \bar{g}_\alpha)}{\bar{g}_\beta + Q_{\alpha\beta}} - \delta_{\alpha\beta} \qquad (5.20)$$

where the matrix $Q_{\alpha\beta}$ is the matrix of dissociation constants of transcription factor $\beta$ on the enhancer of gene $\alpha$. If we just add one continuous parameter $Q_{\alpha\beta} = Q$ (assuming that all four dissociation constants are equal), the agreement between the models **A**, **B**, **C**, **D** and the data can be made even more impressive. We illustrate this in Fig. 5.6 for model **D**.
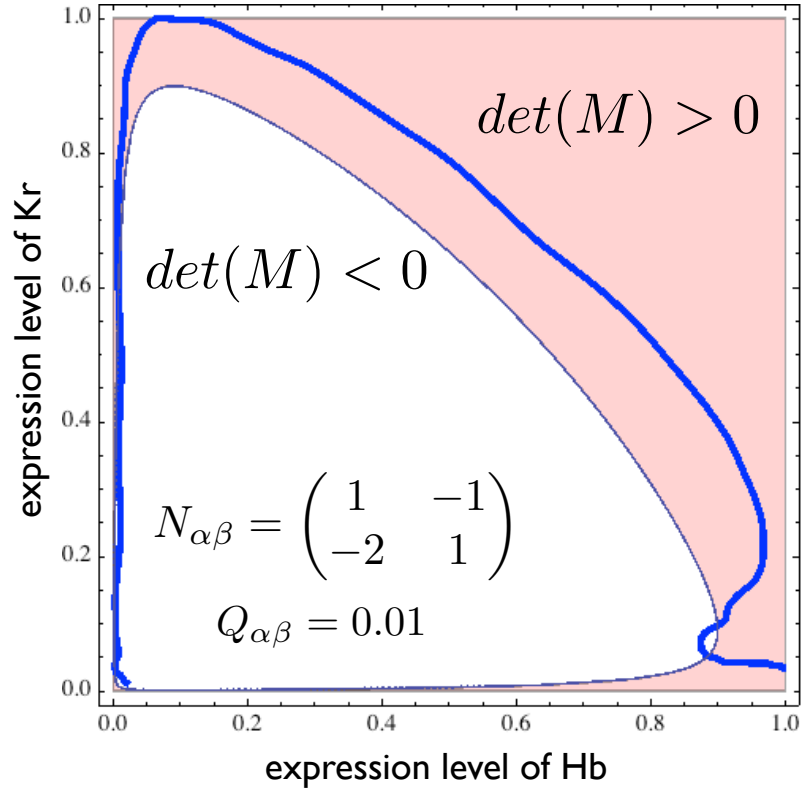
Figure 5.6: The trajectory of Krüppel vs Hunchback expression levels along the anterior–posterior axis of the embryo (blue) superimposed on the region of stability (pink), defined by $det(M) > 0$, and the region of instability (white), defined by $det(M) < 0$. The two regions are separated by the critical surface. This plot is produced for model **D** with equal values of all four dissociation constants $Q_{\alpha\beta} = 0.01$. Compared to the strong binding limit, the regions of stability at small concentrations of transcription factors appear at finite $Q$. The agreement between the model and the data can be further improved by choosing different dissociation constants for all transcription factors.

## 5.5 Conclusions

When we think about the possibility of tuning a genetic network to criticality our naive expectation would be that it is a very difficult thing to do, since the critical surface is always a surface of co-dimension one in the space of parameters of our models. The main result of this chapter is that this intuition is actually wrong, and that given the experimental mean field profiles of expression and our prior knowledge about the architecture of enhancers, there are plenty of critical models in the experimentally relevant window of parameters. All this is valid of course through the lens of a simple physical MWC model for the binding events of transcription factors. It is also worth emphasizing the striking similarity of the critical surfaces for models of Table 5.1 with the experimental profiles, Fig. 5.5, 5.6.

# Chapter 6

# Conclusion

In this chapter we will briefly discuss some future directions of research suggested by the results discussed in the main chapters.

In relation to the de Sitter project perhaps the biggest challenge is to write a general renormalization group equation that can be applied to any initial state both in the Poincare patch and the complete de Sitter space. The question was partly addressed in the Poincare patch for a specific initial condition - the Bunch-Davies vacuum [22]. In principle one can imagine alternative setups. For example, we can start not from an empty space, but from a space with some small initial occupation numbers. Even in the Poincare patch the loop diagrams have interference terms in this situation that are absent in the case of the Bunch-Davies vacuum. It would be interesting to see if these interference contributions can produce any physical effects.

Another interesting direction is to explore alternative (not Bunch-Davies) vacua. For example in the case of the complete de Sitter space the in-in vacuum is different from the Bunch-Davies one. It would be interesting to see if this in-in initial state can produce any new effects in loop calculations.

In relation to the criticality project one immediate question is how patterns of correlations differ in mutant flies. By doing genetic manipulations one can modify

the architecture of the gap gene network. A variety of modifications are possible. One can knock out one of the maternal morphogens, or one of the gap genes, or even make a fruit fly that expresses a gap protein that is disfunctional (i.e. with a mutagenized binding domain). All these modifications of the wild-type genetic network should influence the pattern of correlations that we have observed in the wild-type. By analyzing these alterations of correlations we can further improve our understanding of the interactions between various transcription factors within the network.

Another hope is that one of these mutants will not show any signatures of criticality at all. In this case, we might be able to say how the developmental process is altered in this mutant compared to the normal wild type fruit fly. This might help to identify precisely the role of criticality in development.

A separate question is about the the origin of fine-tuning in this system. The pattern of correlations that was observed in [27] suggests that the regulatory network responsible for producing this pattern is non-generic, meaning that the parameters of this network are tuned to certain values. What kind of biological function might this fine tuning be designed for? One promising possibility is that it may be used for the scaling of the gene expression pattern with the size of the embryo. As we saw in the previous chapters, the fluctuations of expression levels of different genes turn out to be strongly correlated over a large distance in space. Such long-range correlations provide a conceptual possibility for how the information about boundary conditions imposed at the ends of the embryo can propagate sufficiently deep inside the egg (far away from the boundary) to allow the pattern of morphogenic gradients to adjust to variations in the overall size of the embryo. It would be nice to investigate this possibility and more generally establish a relationship between the patterns of correlations and the problem of biological scaling.

# Bibliography

[1] Maximino Aldana, Susan Coppersmith, and Leo P Kadanoff. Boolean dynamics with random couplings. In *Perspectives and Problems in Nolinear Science*, pages 23–89. Springer, 2003.

[2] Per Bak. *How nature works*. Oxford university press Oxford, 1997.

[3] William Bialek. *Biophysics: searching for principles*. Princeton University Press, 2012.

[4] William Bialek, Andrea Cavagna, Irene Giardina, Thierry Mora, Oliver Pohl, Edmondo Silvestri, Massimiliano Viale, and Aleksandra M Walczak. Social interactions dominate speed control in poising natural flocks near criticality. *Proceedings of the National Academy of Sciences*, 111(20):7212–7217, 2014.

[5] Lacramioara Bintu, Nicolas E Buchler, Hernan G Garcia, Ulrich Gerland, Terence Hwa, Jané Kondev, and Rob Phillips. Transcriptional regulation by the numbers: models. *Current opinion in genetics & development*, 15(2):116–124, 2005.

[6] Nicholas David Birrell and Paul Charles William Davies. *Quantum fields in curved space*. Number 7. Cambridge university press, 1984.

[7] Timothy S Bunch and Paul CW Davies. Quantum field theory in de sitter space: renormalization by point-splitting. *Proceedings of the Royal Society of London. A. Mathematical and Physical Sciences*, 360(1700):117–134, 1978.

[8] NA Chernikov and EA Tagirov. Quantum theory of scalar field in de sitter spacetime. In *Annales de l'institut Henri Poincaré (A) Physique théorique*, volume 9, pages 109–141. Gauthier-villars, 1968.

[9] Wolfgang Driever and Christiane Nüsslein-Volhard. The bicoid protein is a positive regulator of hunchback transcription in the early drosophila embryo. *Nature*, 337(6203):138–143, 1989.

[10] Wolfgang Driever, Gudrun Thoma, and Christiane Nüsslein-Volhard. Determination of spatial domains of zygotic gene expression in the drosophila embryo by the affinity of binding sites for the bicoid morphogen. *Nature*, 340(6232):363–367, 1989.

[11] Julien O Dubuis, Reba Samanta, and Thomas Gregor. Accurate measurements of dynamics and reproducibility in small genetic networks. *Molecular systems biology*, 9(1), 2013.

[12] Julien O Dubuis, Gašper Tkačik, Eric F Wieschaus, Thomas Gregor, and William Bialek. Positional information, in bits. *Proceedings of the National Academy of Sciences*, 110(41):16301–16308, 2013.

[13] Timothy S Gardner, Charles R Cantor, and James J Collins. Construction of a genetic toggle switch in escherichia coli. *Nature*, 403(6767):339–342, 2000.

[14] Ulrike Gaul and Detlef Weigel. Regulation of krüppel expression in the anlage of the malpighian tubules in the drosophila embryo. *Mechanisms of development*, 33(1):57–67, 1990.

[15] John Gerhart, Marc Kirschner, and Eileen Starr Moderbacher. *Cells, embryos, and evolution: Toward a cellular and developmental understanding of phenotypic variation and evolutionary adaptability.* Blackwell Science Malden, MA, 1997.

[16] Jeff Hasty, David McMillen, Farren Isaacs, and James J Collins. Computational studies of gene regulatory networks: in numero molecular biology. *Nature Reviews Genetics*, 2(4):268–279, 2001.

[17] Michael Hoch, C Schröder, Eveline Seifert, and H Jäckle. cis-acting control elements for krüppel expression in the drosophila embryo. *The EMBO journal*, 9(8):2587, 1990.

[18] Michael Hoch, Eveline Seifert, and H Jäckle. Gene expression mediated by cis-acting sequences of the krüppel gene in response to the drosophila morphogens bicoid and hunchback. *The EMBO journal*, 10(8):2267, 1991.

[19] Herbert Jäckle, Diethard Tautz, Reinhard Schuh, Eveline Seifert, and Ruth Lehmann. Cross-regulatory interactions among the gap genes of drosophila. 1986.

[20] Johannes Jaeger. The gap gene network. *Cellular and Molecular Life Sciences*, 68(2):243–274, 2011.

[21] Johannes Jaeger, Svetlana Surkova, Maxim Blagov, Hilde Janssens, David Kosman, Konstantin N Kozlov, et al. Dynamic control of positional information in the early drosophila embryo. *Nature*, 430(6997):368–371, 2004.

[22] Dileep P. Jatkar, Louis Leblond, and Arvind Rajaraman. On the Decay of Massive Fields in de Sitter. *Phys.Rev.*, D85:024047, 2012.

[23] Stuart A. Kauffman. *The origins of order: Self-organization and selection in evolution.* Oxford university press, 1993.

[24] LV Keldysh. Diagram technique for nonequilibrium processes. *Sov. Phys. JETP*, 20(4):1018–1026, 1965.

[25] Yoosik Kim, Antonina Iagovitina, Keisuke Ishihara, Kate M Fitzgerald, Bart Deplancke, Dmitri Papatsenko, and Stanislav Y Shvartsman. Context-dependent transcriptional interpretation of mitogen activated protein kinase signaling in the drosophila embryo. *Chaos: An Interdisciplinary Journal of Nonlinear Science*, 23(2):025105, 2013.

[26] Dmitry Krotov and William Bialek. The Monod–Wyman–Changeux model of the gap gene network. *Unpublished*, 2013.

[27] Dmitry Krotov, Julien O Dubuis, Thomas Gregor, and William Bialek. Morphogenesis at criticality. *Proceedings of the National Academy of Sciences*, 111(10):3683–3688, 2014.

[28] Dmitry Krotov and Alexander M. Polyakov. Infrared Sensitivity of Unstable Vacua. *Nucl.Phys.*, B849:410–432, 2011.

[29] Peter Anthony Lawrence et al. *The making of a fly: the genetics of animal design.* Blackwell Scientific Publications Ltd, 1992.

[30] Thomas Lecuit, Reba Samanta, and Eric Wieschaus. Slam encodes a developmental regulator of polarized membrane growth during cleavage of the drosophila embryo. *Developmental cell*, 2(4):425–436, 2002.

[31] Xiao-yong Li, Stewart MacArthur, Richard Bourgon, David Nix, Daniel A Pollard, Venky N Iyer, Aaron Hechmer, Lisa Simirenko, Mark Stapleton, Cris L Luengo Hendriks, et al. Transcription factors bind thousands of active and inactive regions in the drosophila blastoderm. *PLoS biology*, 6(2):e27, 2008.

[32] Feng Liu, Alexander H Morrison, and Thomas Gregor. Dynamic interpretation of maternal inputs by the drosophila segmentation gene network. *Proceedings of the National Academy of Sciences*, 110(17):6724–6729, 2013.

[33] Marcelo O Magnasco, Oreste Piro, and Guillermo A Cecchi. Self-tuned critical anti-hebbian networks. *Physical review letters*, 102(25):258102, 2009.

[34] Donald Marolf and Ian A. Morrison. The IR stability of de Sitter QFT: Physical initial conditions. *Gen.Rel.Grav.*, 43:3497–3530, 2011.

[35] Jacque Monod, Jeffries Wyman, and Jean-Pierre Changeux. On the nature of allosteric transitions: a plausible model. *Journal of molecular biology*, 12(1):88–118, 1965.

[36] Thierry Mora and William Bialek. Are biological systems poised at criticality? *Journal of Statistical Physics*, 144(2):268–302, 2011.

[37] Thierry Mora, Aleksandra M Walczak, William Bialek, and Curtis G Callan. Maximum entropy models for antibody diversity. *Proceedings of the National Academy of Sciences*, 107(12):5405–5410, 2010.

[38] N.B. Narozhnyi and A.I. Nikishov. The Simplist processes in the pair creating electric field. *Yad.Fiz.*, 11:1072, 1970.

[39] Christiane Nüsslein-Volhard and Eric Wieschaus. Mutations affecting segment number and polarity in drosophila. *Nature*, 287(5785):795–801, 1980.

[40] A.M. Polyakov. De Sitter space and eternity. *Nucl.Phys.*, B797:199–217, 2008.

[41] A.M. Polyakov. Decay of Vacuum Energy. *Nucl.Phys.*, B834:316–329, 2010.

[42] A.M. Polyakov. Infrared instability of the de Sitter space. 2012.

[43] Mike Rothe, Ernst A Wimmer, Michael J Pankratz, Marcos González-Gaitán, and Herbert Jäckle. Identical transacting factor requirement for knirps and knirps-related gene expression in the anterior but not in the posterior region of the drosophila embryo. *Mechanisms of development*, 46(3):169–181, 1994.

[44] Julian Schwinger. Brownian motion of a quantum oscillator. *Journal of Mathematical Physics*, 2(3):407–432, 1961.

[45] Gasper Tkacik, Thierry Mora, Olivier Marre, Dario Amodei, II Berry, J Michael, and William Bialek. Thermodynamics for a network of neurons: Signatures of criticality. *arXiv preprint arXiv:1407.5946*, 2014.

[46] Gašper Tkačik, Aleksandra M Walczak, and William Bialek. Optimizing information flow in small genetic networks. iii. a self-interacting gene. *Physical Review E*, 85(4):041903, 2012.

[47] Jessica Treisman and C Desplan. The products of the drosophila gap genes hunchback and kruppel bind to the hunchback promoters. *Nature (London)*, 341:335–337, 1989.

[48] Alan Mathison Turing. The chemical basis of morphogenesis. *Philosophical Transactions of the Royal Society of London. Series B, Biological Sciences*, 237(641):37–72, 1952.

[49] Ernst A Wimmer, Alan Carleton, Phoebe Harjes, Terry Turner, and Claude Desplan. Bicoid-independent formation of thoracic segments in drosophila. *Science*, 287(5462):2476–2479, 2000.

[50] Lewis Wolpert. Positional information and the spatial pattern of cellular differentiation. *Journal of theoretical biology*, 25(1):1–47, 1969.